

AD-A145 506

RELATIONSHIPS BETWEEN ELECTRONIC STRUCTURE AND
STABILITY OF METALLIC GLAS. (U) PARIS-6 UNIV (FRANCE)
LABORATOIRE D'OPTIQUE DES SOLIDES F ABELES ET AL.

1/1

UNCLASSIFIED

JUN 84 AFOSR-TR-84-0705 AFOSR-83-0060

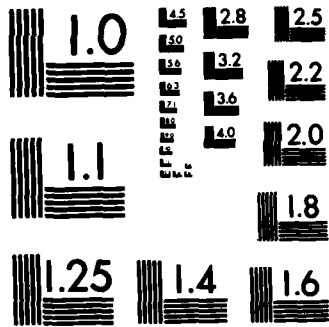
F/G 20/12

NL

END

FILED

DTIC



MICROCOPY RESOLUTION TEST CHART
NATIONAL BUREAU OF STANDARDS-1963-A

AFOSR-TR- 84-0705

4

Grant number : AFOSR 83-00-60

RELATIONSHIPS BETWEEN ELECTRONIC STRUCTURE AND STABILITY OF METALLIC GLASSES

F. Abelès
M.L. Thèye
V. Nguyen Van

Laboratoire d'Optique des Solides,
Université Pierre et Marie Curie
4, place Jussieu, 75230 PARIS Cédex 05,
FRANCE

June 1984

SDTIC
ELECTE
SEP 10 1984
A

Final Scientific Report, 1 January 1983 - 31 December 1983

Approved for public release ; distribution unlimited

Prepared for

United States Air Force, Air Force Office of Scientific Research,
Building 410, Bolling AFB, D.C. 20332, U.S.A.

and

European Office of Aerospace Research and Development, London, England.

AD-A145 506

DTIC FILE COPY

84 08 30 036

66

REPORT DOCUMENTATION PAGE		READ INSTRUCTIONS BEFORE COMPLETING FORM
1. REPORT NUMBER AFOSR-TR. 84-0705	2. GOVT ACCESSION NO. A145506	3. RECIPIENT'S CATALOG NUMBER
4. TITLE (and Subtitle) RELATIONSHIPS BETWEEN ELECTRONIC STRUCTURE AND STABILITY OF METALLIC GLASSES		5. TYPE OF REPORT & PERIOD COVERED Final scientific Report 1 Janv. 1983 - 31 Dec. 1983
7. AUTHOR(s) F. Abelès M.L. Thèye V. Nguyen Van		6. PERFORMING ORG. REPORT NUMBER
9. PERFORMING ORGANIZATION NAME AND ADDRESS Laboratoire d'Optique des Solides Université Pierre et Marie Curie 4, place Jussieu, 75230 PARIS Cédex 05, FRANCE		8. CONTRACT OR GRANT NUMBER(s) AFOSR-83-0060
11. CONTROLLING OFFICE NAME AND ADDRESS AFOSR/NE 2149410 Bolling Hq B DC 20332		10. PROGRAM ELEMENT, PROJECT, TASK AREA & WORK UNIT NUMBERS 61102F 2306C3
14. MONITORING AGENCY NAME & ADDRESS (if different from Controlling Office)		12. REPORT DATE June 1984
		13. NUMBER OF PAGES 38
		15. SECURITY CLASS. (of this report) UNCLASSIFIED
		15a. DECLASSIFICATION/DOWNGRADING SCHEDULE
16. DISTRIBUTION STATEMENT (of this Report) Approved for public release Approved for public release; distribution unlimited.		
17. DISTRIBUTION STATEMENT (of the abstract entered in Block 20, if different from Report) Distribution unlimited		
18. SUPPLEMENTARY NOTES		
19. KEY WORDS (Continue on reverse side if necessary and identify by block number) amorphous metallic alloys, co-evaporation, electrical resistivity, optical properties, Drude model.		
20. ABSTRACT (Continue on reverse side if necessary and identify by block number) Amorphous MgZn alloys have been obtained in the form of thin films by co-evaporation under ultra-high vacuum on cold sapphire substrates (300K) for Zn concentrations between 25 and 35 at.%. These films crystallize at about 350K. Their d.c. electrical resistivity and their optical properties between 0.6 and 4 eV have been investigated in situ. The resistivity versus temperature behaviour is roughly similar to that reported for quenched bulk alloys but the resistivity		

Gov. 1)

(... 14K)

20.

values are significantly larger. The complex dielectric constant follows the free-electron Drude model at low energies up to 1.8 eV. The optical free electron parameters are discussed and compared to those obtained on other free-electron-like amorphous alloys. Special attention is paid to the average effective number of conduction electrons per atom, which is found to be smaller than expected. ←

1. Introduction

Metallic glasses form an interesting class of new materials, not only because of their unique properties which make them suitable for various applications, but also because they offer a possibility of testing the theoretical models proposed for the effects of topological disorder in metals. Although most studies have up to now been devoted to systems involving transition metals, amorphous alloys containing only "normal", i.e. free-electron-like metals, like the amorphous Mg-Zn alloys, presently attract more and more interest. This is largely due to the expected relative simplicity of their electronic structure, since the conduction electron states can be assumed to be almost exclusively of s and p character. Such a case can be treated theoretically by ab initio pseudo-potential methods (1-4), which succeeded in explaining the constitution diagrams as well as the inter-relation between glass formation and phase diagram from a microscopic quantum-mechanical basis. It has been shown that the bonding in all stable phases arises from an optimal embedding of the neighbouring atoms into the attractive minima of the interatomic pair potentials, which means, for disordered phases, the matching between the minima in the pair potentials and the maxima in the partial pair distribution functions. The geometrical basis is always tetrahedral close packing of the atoms ; this leads, either to Frank-Kasper phases for a majority concentration of smaller atoms (Zn in the MgZn case), or to random tetrahedral packing based on icosahedral micro-units for a majority concentration of the larger atoms (Mg in the MgZn case)(3). Besides, these amorphous alloys are of significant importance from the point of view of the electron transport properties. They have indeed relatively low resistivities (of the order of 50-100 $\mu\Omega\text{cm}$), which makes them particularly suited for tests of theories based on the Faber-Ziman theory, initially developed for liquid metals on the basis of the nearly-free-electron model and the use of the pseudopotential concept, under the assumption of weak scattering, and later on generalized to amorphous metallic alloys (5-10).

Amorphous MgZn alloys have first been obtained by rapid quenching from the melt in a narrow composition range around the deep eutectic ($\text{Mg}_{72}\text{Zn}_{28}$) : $25 < x_{\text{Zn}} < 32$ at.% (11). This range has later on been somewhat extended, using the same melt-spinning technique : $22,5 < x_{\text{Zn}} < 35$ at.% (12). Amorphous MgZn alloys have also been prepared in the form of thin films by a getter-sputtering technique on substrates maintained at 77K, over a much wider composition range : $10 < x_{\text{Zn}} < 90$ at.% ; however, the results of transport measurements on these films are strongly scattered, which may indicate that all samples are not homogeneous (13).

The structure of amorphous MgZn alloys has been investigated by neutron (12,14) and X-ray (11,15) diffraction. Both the interference functions $S(q)$ and the pair correlation functions $G(r)$ agree quite well with those obtained by a relaxed dense random packing of hard sphere model with realistic pseudopotentials and periodic boundary conditions (16), although the experimental peaks are lower than those in the model. The first peak in the interference function (or total structure factor) is located at $q_1 = 2.62 - 2.65 \text{ \AA}^{-1}$ for $\text{Mg}_{70}\text{Zn}_{30}$; its position slightly shifts to larger q values with increasing Zn concentration (12). The second maximum presents a well-pronounced splitting. The prepeak which has been noticed in several X-ray diffraction experiments at $q = 1.54 \text{ \AA}^{-1}$ has been interpreted as reflecting the existence of chemical short-range order in the amorphous alloys (15,17) ; the spatial extension of this short-range ordering is however believed to be rather small : 8 \AA (15). The amorphous MgZn alloys crystallize slightly above room temperature (11,18,19). The crystallization process consists in two successive steps, in which the atoms take first the short-range order, second the long-range order of the crystalline phase $\text{Mg}_{51}\text{Zn}_{20}$.

The transport properties of amorphous MgZn alloys prepared by rapid quenching from the melt, have been studied in detail over a wide temperature range (13, 20-23). The results of Hall effect (21), electronic specific heat (24), magnetic susceptibility (25) and Compton profile (26) measurements all reveal remarkably good agreement with the predictions of a free-electron model, with Mg

and Zn both contributing two electrons per atom to the alloy conduction band. There is however some composition dependence of several of these physical quantities, especially in the vicinity of the composition of the crystalline phase $Mg_{51}Zn_{20}$ ($x_{Zn} = 28.2$ at.%) (12).

The aim of the present work was to prepare amorphous MgZn alloys in the form of thin films by co-evaporation of the two constituents under ultra-high vacuum onto substrates maintained at low temperature, to measure their transport and optical properties in situ as a function of temperature, and to compare the results to those reported for bulk quenched amorphous alloys. Co-evaporation under ultra-high vacuum presents the advantage of avoiding contamination of the samples during their preparation, the two metal constituents, especially Mg, being highly oxidizable materials. It also allows to obtain thin films with high-quality surfaces, well adapted to precision optical measurements. The optical properties of amorphous MgZn alloys have never been investigated up to now. Such studies are complementary to those of the transport properties, since they can give information on the conduction-electron behaviour in the presence of a high-frequency electromagnetic field ; they are particularly useful in that respect since they allow to determine the ratio of the average effective number of electrons per atom n to their effective mass m , and the relaxation time τ separately, while d.c. electrical resistivity measurements only yield the product of these quantities. Optical studies can on the other hand bring some insight into the electronic density of states, by revealing the existence of interband electron transitions (27-29).

We present in the following the results obtained on a series of amorphous $Mg_{1-x}Zn_x$ alloy films, with $26 < x_{Zn} < 35$ at.%, all measurements being performed in situ, under ultra-high vacuum. In section 2, we briefly describe the experimental set-up, the deposition conditions, and the different experimental techniques. In section 3, we investigate the variations of the electrical d.c. resistivity as a function of temperature between 10 and 300K, and we analyse in detail, on the one hand the irreversible effects occurring during annealing of the as-deposited films up to 300K, on the other hand,

the reversible behaviour of the resistivity for annealed (stabilized) amorphous samples. In section 4, we examine the optical properties as deduced from in situ reflectance and transmittance measurements from 0.6 to 4 eV on as-deposited and annealed films, and we analyse these properties in terms of the free-electron Drude model. We discuss the values of the characteristic parameters of the conduction electrons as a function of composition.

2. Preparation and characterization of amorphous MgZn alloys

We use a special ultra-high vacuum experimental set-up which allows to prepare the films by controlled co-evaporation on substrates maintained at low temperature and to measure their optical properties (reflectance R and transmission T) and their d.c. electrical resistance in situ between 10 and 370 K (30). The base pressure in the experimental chamber is of the order of 10^{-9} Torr, and remains smaller than $5 \cdot 10^{-8}$ Torr during evaporation. The evaporation rates from the two separate crucibles are controlled by two calibrated quartz-microbalances coupled with an Apple II Plus minicomputer ; a feed-back process allows to monitor the heating of each crucible in order to keep constant the ratio of the deposition rates of the two constituents. Both the composition and the average mass thickness of the films can thus be determined with an uncertainty of $\pm 1\%$. The total deposition rate is in all cases of the order of $10 \text{ \AA}/\text{sec}$. The alloy composition is checked by an α -particle back-scattering technique (31) ; the agreement with the quartz-microbalance indications is quite good, within a few %. The problem of the actual film thickness proved to be more difficult to solve. Due to the very rapid oxidization of the films when submitted to ambient atmosphere, making any measurement impossible outside the vacuum chamber, we could not apply our usual X-ray interference technique (32) for determining the film thickness ; the fringe system was indeed strongly modified by the presence of an oxide layer. The

average mass thickness d_Q defined as $d_Q = d_{Mg} + d_{Zn}$, d_{Mg} and d_{Zn} being given by the respective quartzmicrobalances (assuming that the density D is equal to 1.74 and 7.14 g/cm³ for pure Mg and pure Zn), would correspond to an alloy with a density D_{av} equal to :

$$D_{av} = \frac{d_{Mg}D_{Mg} + d_{Zn}D_{Zn}}{d_{Mg} + d_{Zn}}$$

i.e.

$$D_{av} = D_{Mg}D_{Zn} \frac{M_{Mg}x_{Mg} + M_{Zn}x_{Zn}}{M_{Mg}D_{Zn}x_{Mg} + M_{Zn}D_{Mg}x_{Zn}}$$

if M_{Mg} and M_{Zn} are the Mg and Zn molecular weights, and x_{Mg} and x_{Zn} the Mg and Zn atomic concentrations ($x_{Mg} = 1 - x_{Zn} = 1 - x$) respectively. Figure 1 shows the variation of this "average" density D_{av} with Zn atomic concentration x . The experimental values for bulk quenched amorphous MgZn alloys obtained by Matsuda and Mizutani (12) are also reported on this figure ; the variation with x is identical, but the values are larger than the predicted ones : $\Delta D/D_{av} \approx 2.7\%$. Unfortunately, we do not know the actual density of our films. We have tried to determine their "optical" thickness from the in situ reflectance and transmittance measurements only, by two different methods. The first one consists in considering the thickness as an additional adjustable parameter when fitting the near infra-red data to the Drude model, as explained in section 4. The second one is based on a Kramers-Kronig analysis of the reflectance data. We know that the phase change on reflection θ_R at one frequency ω can be obtained from the whole reflectance spectra $R(\omega')$ through the relation :

$$\theta_R(\omega) = - \frac{\omega}{\pi} \mathcal{P} \int_0^{\infty} \frac{\text{Log } R(\omega')}{\omega'^2 - \omega^2} \cdot d\omega'$$

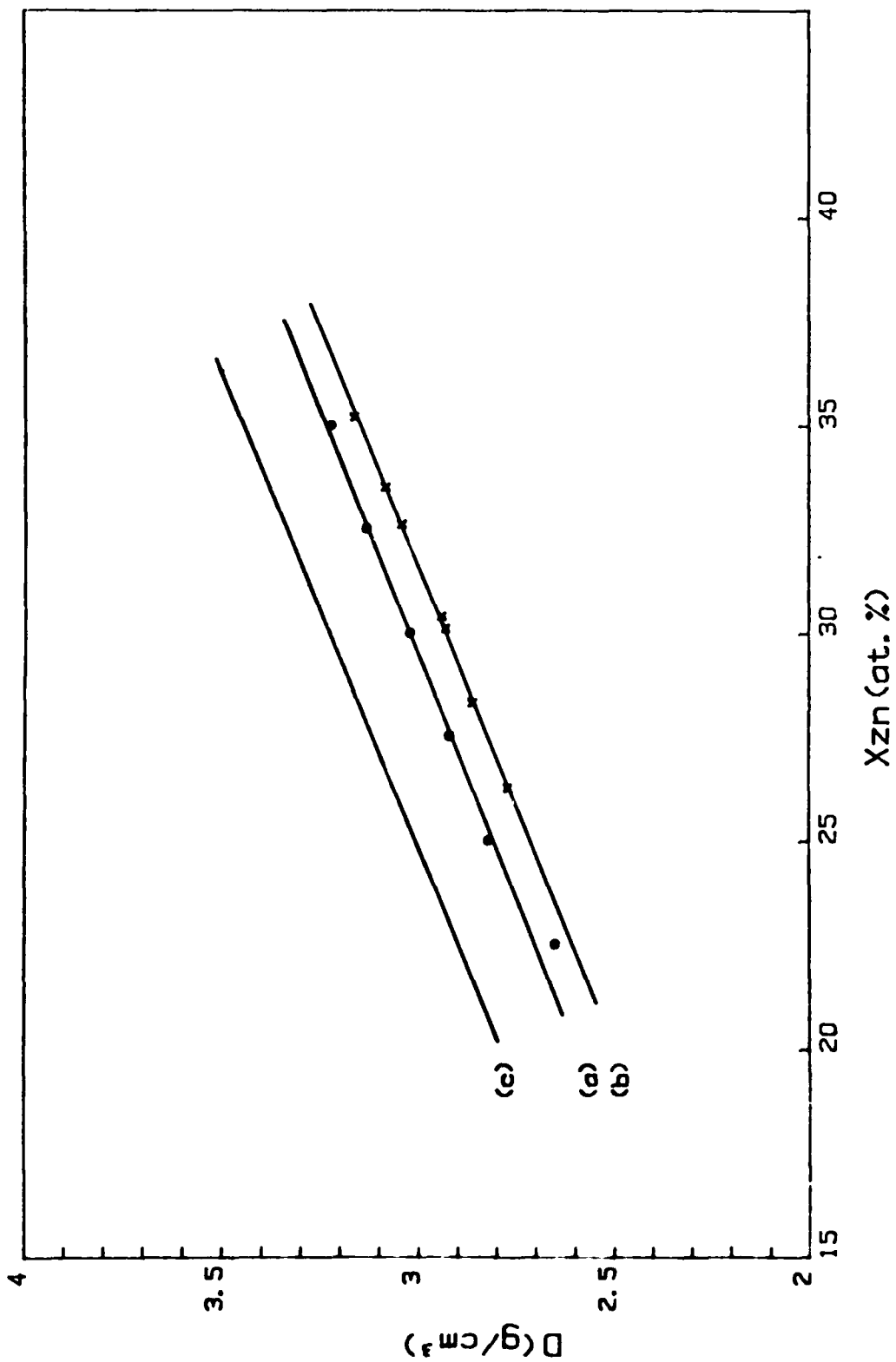


Figure 1 : Density of amorphous MgZn alloys versus Zn concentration x_{Zn} : for quenched alloys, from ref. 12 (a) ; for co-evaporated alloy films, if the film thickness is taken equal to the average mass thickness d_Q : Day (b) or to the "optical" thickness d_{allo} : Dalloy (c).

We can only compute that part of the integral between ω_1 and ω_H , which are the extreme points of the spectral range of measurement, i.e. :

$$\theta_R^{ex}(\omega) = -\frac{\omega}{\pi} \int_{\omega_1}^{\omega_H} \frac{\log R(\omega')}{\omega'^2 - \omega^2} d\omega'$$

We then assume that the rest of the integral can be approximated by an expression of the form : $A\omega^{-1} + B$

so that : $\theta_R(\omega) = \theta_R^{ex}(\omega) + A\omega^{-1} + B$

The method consists in writing the systems of three equations :

$$R(n, k, d, \omega) = R_{ex}$$

$$T(n, k, d, \omega) = T_{ex}$$

$$\delta_R(n, k, d, \omega) = \theta_R^{ex} + A\omega^{-1} + B$$

(R , T and δ_R being exact thin film formulas (33) and R_{ex} , T_{ex} the experimental reflectance and transmittance values) for three consecutive values of the frequency ω_{i-1} , ω_i , ω_{i+1} . If we assume that the A and B coefficients retain approximately the same values for the three frequencies considered, one obtains in this way 9 equations for only 9 unknowns : the optical constants n_{i-1} , k_{i-1} , n_i , k_i , n_{i+1} , k_{i+1} , the thickness d , and the coefficients A and B ; this system is solved by a least-square fitting procedure. Although neither method gives a unique and satisfactory result in all cases, the "optical" thickness values which we have obtained in a few favourable cases indicate that the density of our co-evaporated amorphous films must be slightly larger than that of bulk quenched samples : $\Delta D/D_{av} \approx 5\%$. This assumed density D_{alloy} is reported in figure 1 as a function of Zn atomic concentration. In the following, we will use the average mass thickness d_Q for computing the electrical resistivity and for analysing the optical properties ; we will also systematically employ the value d_{alloy} deduced when assuming $D = D_{alloy}$, in order to estimate the influence of the choice of the film thickness on the determination of the conduction electron parameters.

The film reflectance and transmittance at nearly normal incidence are measured in situ with a special vacuum spectrophotometer, between 0.6 and 4.2 eV (2 and 0.3 μm). The accuracy of these measurements is of the order of 0.1-0.3%, which is absolutely necessary for a reliable analysis of the data. The measurements are performed just after deposition, as well as at different annealing stages if necessary. The complex dielectric constant $\bar{\epsilon} = \epsilon_1 + i\epsilon_2 = (n + ik)^2$ is computed from the R and T values at any wavelength, using exact thin film formulas and taking into account multiple reflections inside the transparent substrate ; the thickness must be known for this procedure (34).

The d.c. electrical resistance is measured versus temperature between 10 and 370 K by a four-point method ; the thermocouples are made of thin AuFe/Chromel wires held in contact with the film surface with two Indium patches. A special differential method, allowing to measure resistance changes as small as $10^{-3} \Omega$ for resistance values greater than 100Ω , is used when the sample resistance varies very little with temperature.

We had planned to investigate the amorphous alloy structure by electron microscopy and electron diffraction, using pieces of the films detached from the substrate with collodion and collected on microscope grids after collodion dissolving. Unfortunately, due to the rapid oxidization of the films at ambient atmosphere, we have up to now been unable to carry such detailed structure studies. We have only checked that the alloy films were still amorphous at room temperature.

3. d.c. electrical resistivity

As far as their d.c. electrical resistivity is concerned, two

different types of samples must be distinguished :

a) the first films were deposited on silica substrates held at a temperature comprised between 15 and 20 K, and were rather thin : 250 to 300 Å. Their resistivity just after deposition is of the order of 105 $\mu\Omega\text{cm}$, irrespective of the composition. When increasing the temperature, ρ begins to decrease until 100-110K, then increases quite strongly, reaches a pronounced maximum around 250K, and drops more or less abruptly when approaching room temperature. The relative variation of the resistivity between its initial value and its maximum value seems to depend both on the film deposition conditions and composition and on the heating rate, but can be as large as 50%. This annealing behaviour is illustrated in figure 2 for a film with $x_{\text{Zn}} = 26$ at.% and $d_Q = 259$ Å. In the absence of any detailed structure study, it is difficult to conclude about the specificity of the as-deposited samples. For most of them, the reflectance and transmittance spectra at deposition temperature exhibit a structure at about 0.9 μm , which is not found for the other type of films ; this structure becomes more pronounced after annealing at 300K. We will assume that these samples are not completely amorphous or homogeneous, or have a peculiar short-range order, and we will not consider them in the following.

b) the other films were deposited onto sapphire substrates maintained at 10K ; the deposition rate was the same as precedingly, but probably more uniform. These films were also thicker, between 500 and 700 Å. Their resistivity just after deposition are smaller than precedingly : between 80 and 90 $\mu\Omega\text{cm}$, and do not vary significantly with the film composition (figure 3). When increasing temperature, ρ remains approximately constant over a small temperature range, up to 30-40K, then decreases slightly, goes through a plateau or a faint maximum around 150-200K, and decreases again slowly above 200K. The total relative variation of the resistivity between 10 and 300K does not exceed 10%. This annealing behaviour is illustrated in figure 2 for a film with $x_{\text{Zn}} = 30.5$ at.% and $d_Q = 600$ Å. We believe

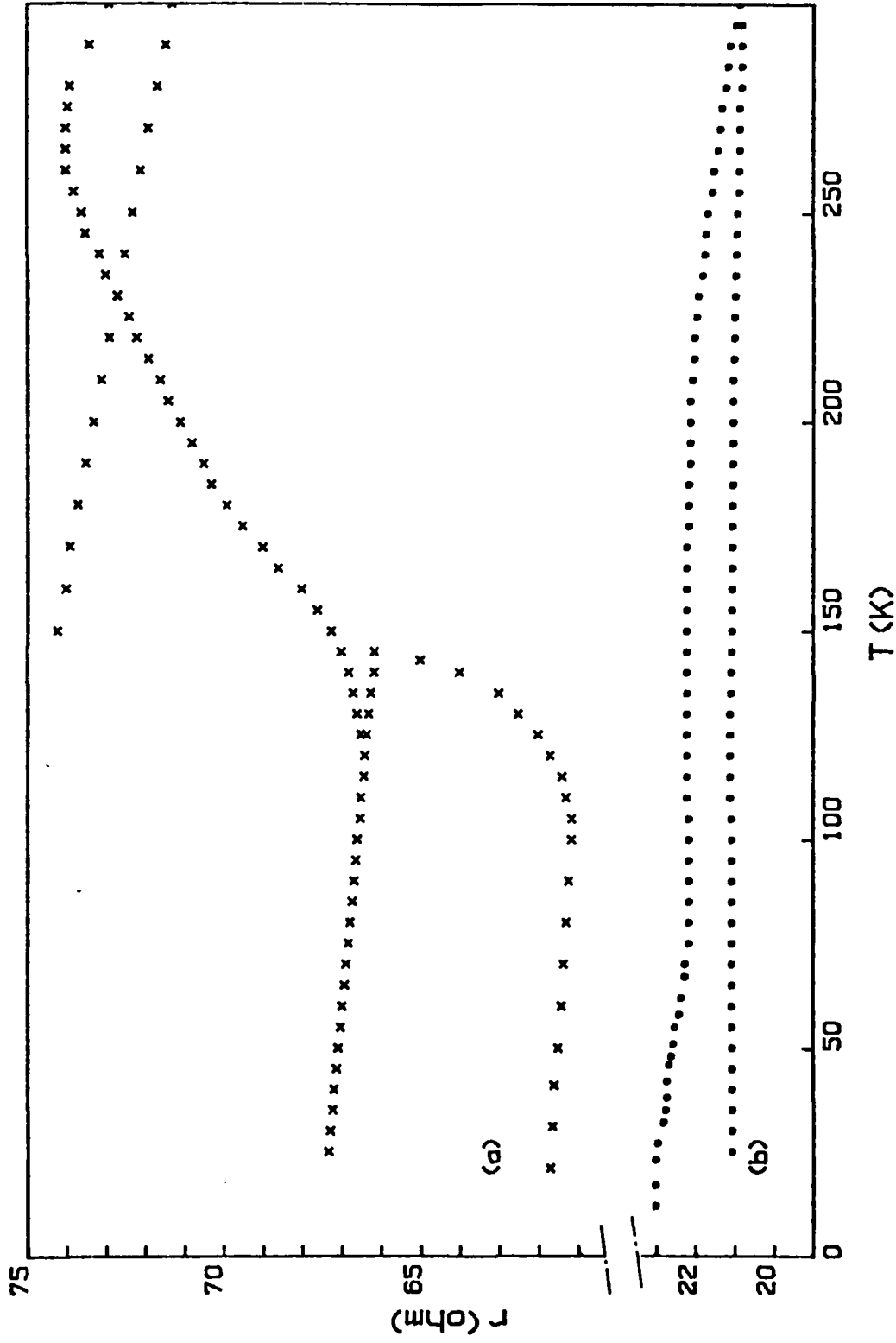


Figure 2 : Variation of the d.c. electrical resistance r with temperature T during annealing from deposition temperature (10-20 K) to room temperature, for amorphous MgZn alloy films deposited in different conditions : (a) $x_{Zn} = 26$ at.%, $d_Q = 259$ Å, silica substrate ; (b) $x_{Zn} = 30.5$ at.%, $d_Q = 600$ Å, sapphire substrate.

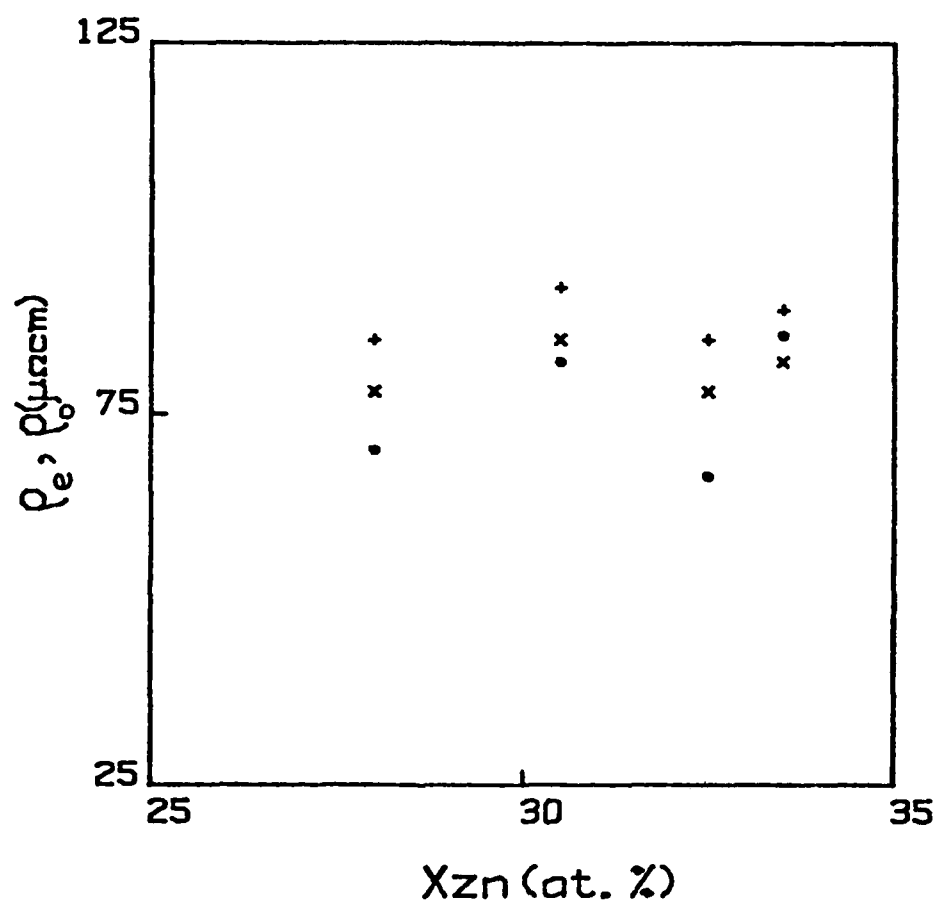


Figure 3 : d.c. electrical resistivity ρ_e computed with the film thickness d equal to d_Q (+) and d_{alloy} (x), and optical resistivity ρ_o deduced from the optical parameters obtained with $d = d_{\text{alloy}}$ (•), for as-deposited co-evaporated amorphous MgZn films with different compositions.

that these samples are truly amorphous over the whole temperature range between 10 and 300K. Crystallization only occurs above room temperature, as shown in figure 4 for a film with $x_{Zn} = 35$ at.% and $d_Q = 614 \text{ \AA}$. The apparition of the $Mg_{51}Zn_{20}$ crystalline phase corresponds to the steep decrease of the resistivity observed between 350 and 360K. This crystallization temperature is in good agreement with those reported for quenched samples (18,35). It can be noticed that the temperature coefficient of the resistivity of the crystalline phase is positive, again in agreement with previous results (18).

The annealing curves between 10 and 300K indicate that, for our co-evaporated amorphous MgZn alloys deposited at low temperature, irreversible relaxation effects occur in several successive steps : a first one starting at quite low temperature (30-40K) and yielding a decrease of the resistivity ; a second one showing up around 150-200K, corresponding on the contrary to a more or less important increase of the resistivity ; a third one at still higher temperatures, giving again a decrease of the resistivity. This last process eventually saturates when the sample is kept at room temperature. The atomic rearrangements taking place during the film relaxation must therefore be rather complicated. It may be worth recalling that studies of the relaxation of bulk quenched alloys above room temperature, just before crystallization onset, by both resistivity measurements and X-ray diffraction experiments (18,35) revealed a relaxation process resulting in an increase of the resistivity, which was interpreted as a change of the short-range order towards that existing in the crystalline $Mg_{51}Zn_{20}$ phase. The interpretation of our data may be different, since we observe such phenomena far from crystallization. Moreover, the short-range order in our co-evaporated samples is certainly somewhat different from that in quenched samples, and probably presents more local fluctuations, especially just after deposition. This may explain the complexity of our $\rho(T)$ curves.

The reversible variation of the resistivity versus temperature between 10 and 300K for amorphous MgZn alloy films stabilized by annealing at room temperature, is shown in a few cases in figure 5. ρ varies very little over the whole temperature range. It starts

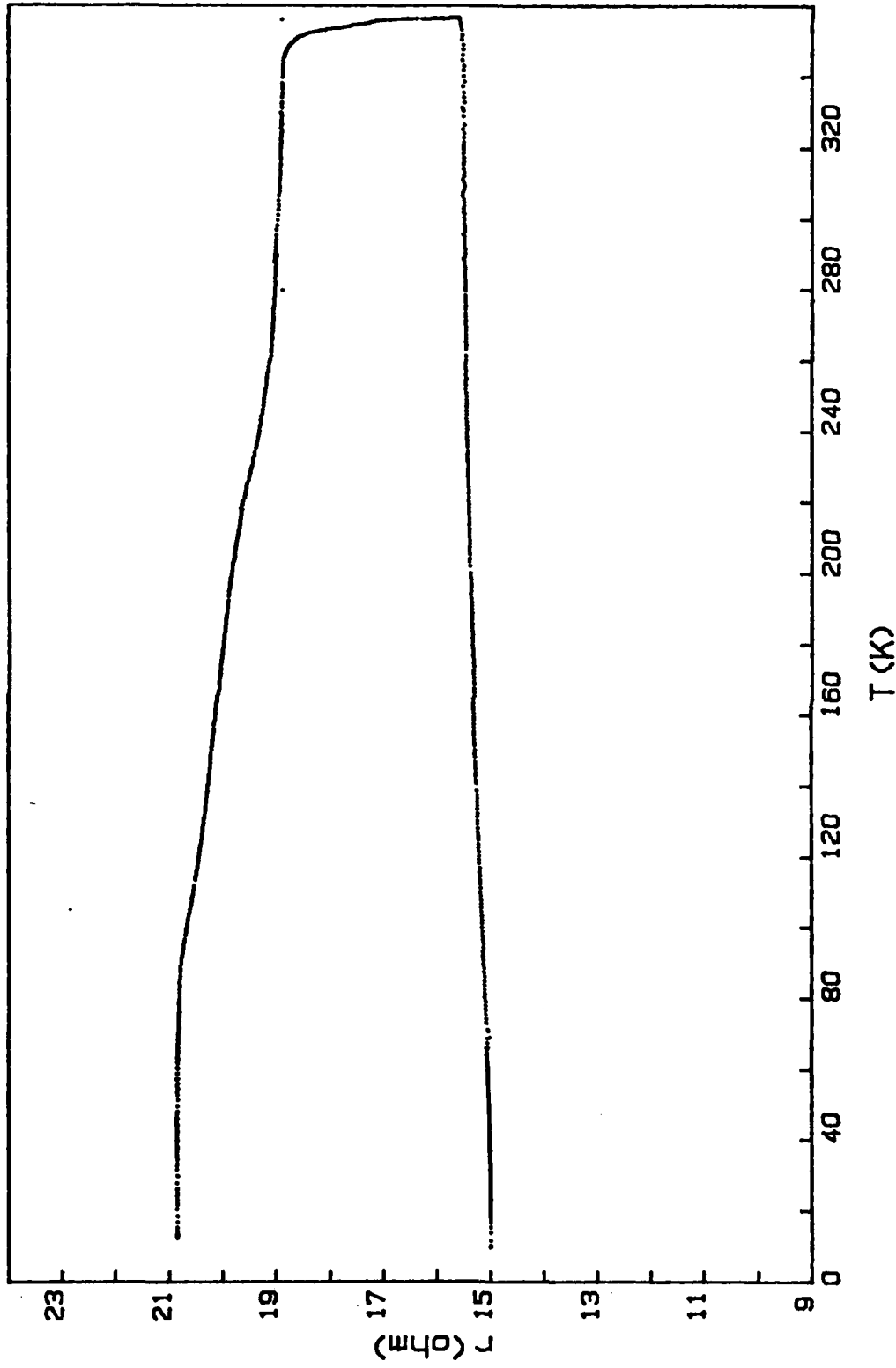


Figure 4 : Variation with temperature T of the d. c. electrical resistance r of an amorphous MgZn alloy film ($x_{Zn} = 35$ at.%, $d_Q = 614 \text{ \AA}$) deposited at 77 K, during annealing until crystallization.

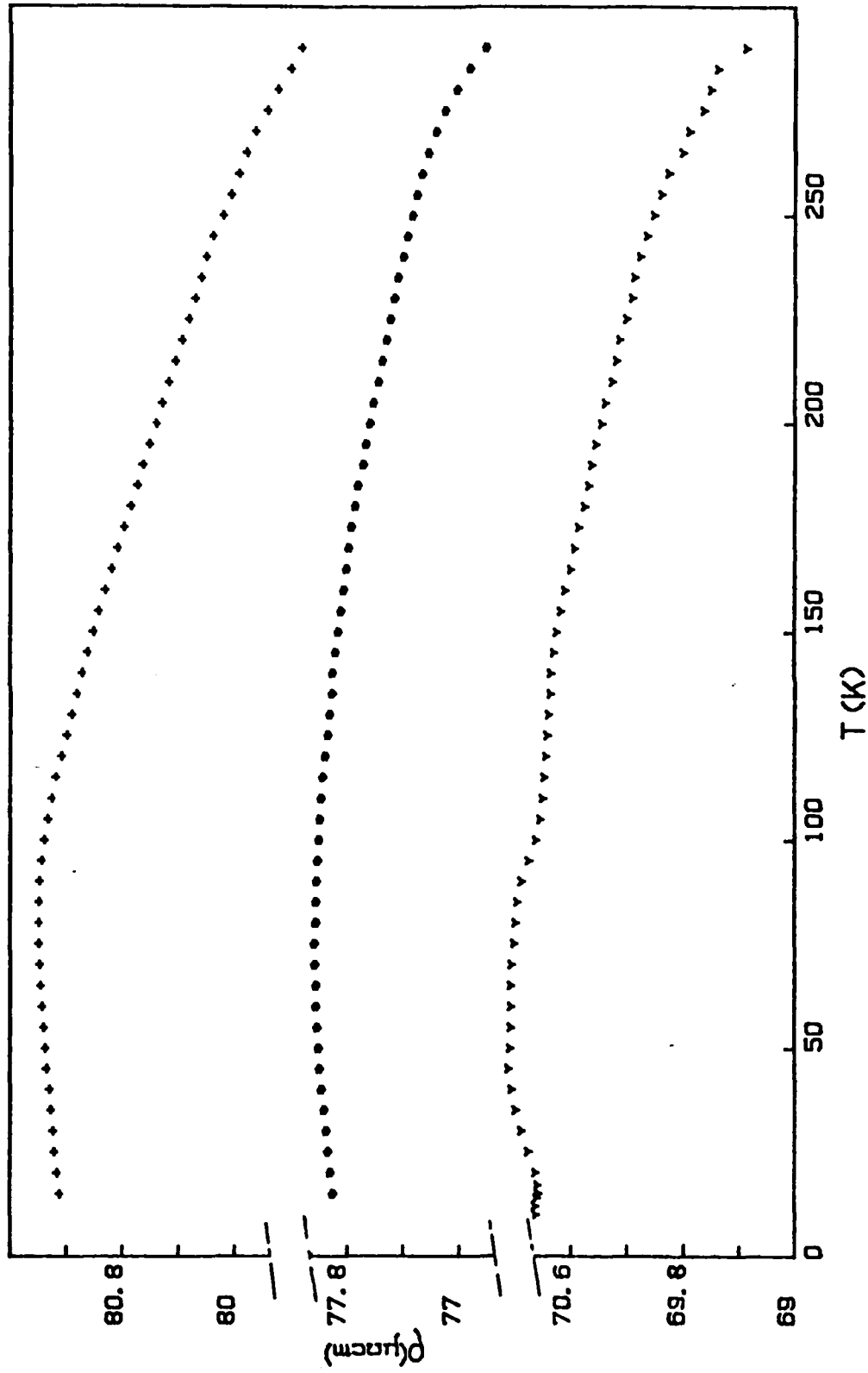


Figure 5 : Reversible variation with temperature T of the d.c. electrical resistivity of co-evaporated amorphous $MgZn$ alloy films deposited at low temperature and annealed at room temperature : (+) $d_Q = 515 \text{ \AA}$, $x_{Zn} = 33.5 \text{ at.}\%$; (♦) $d_Q = 600 \text{ \AA}$, $x_{Zn} = 30.5 \text{ at.}\%$, (▼) $d_Q = 602 \text{ \AA}$, $x_{Zn} = 28 \text{ at.}\%$.

to increase very slightly, goes through a faint, broad maximum, then decreases until room temperature, the variation being approximately linear. The more rapid drop when approaching room temperature for some samples is an irreversible effect, due to the fact that these films were not allowed to relax completely when previously annealed at room temperature. Our results are at least in qualitative agreement with those reported for bulk quenched amorphous alloys (12, 21-23). Our measurements are not going far enough towards low temperatures to detect the shallow minimum around 10K pointed out by Matsuda and Mizutani (21). But we observe the T^2 dependence predicted at low temperatures by extension of the Faber-Ziman theory (9,36) over a small temperature range below the maximum, as well as the empirical law : $\rho = \rho_{\max} - A(T - T_{\max})^{3/2}$ proposed by Matsuda and Mizutani (21) above the maximum, before the approximately linear variation sets in (figure 6). The different quantities characteristic of the resistivity behaviour for our co-evaporated amorphous alloys are summarized in Table I for different compositions. When comparing these results to those reported for quenched alloys, the following remarks can be made :

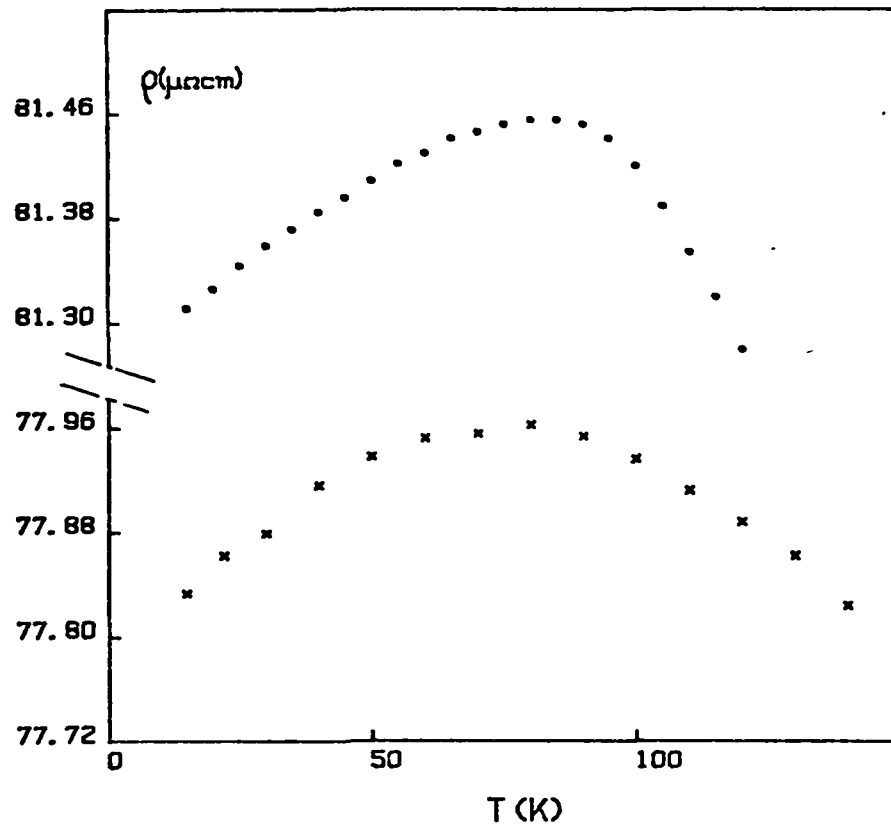
i) the resistivity values are significantly larger than those corresponding to quenched alloys, which are usually comprised between 40 and 60 $\mu\Omega\text{cm}$ (20-24), but smaller than those of co-sputtered films, comprised between 100 and 130 $\mu\Omega\text{cm}$ (13).

ii) the position of the maximum, although varying somewhat from sample to sample irrespective of the composition, seems to be shifted to higher temperatures with respect to quenched samples.

iii) the temperature coefficient of the resistivity near room temperature has somewhat smaller absolute values than in quenched samples.

Several rather sophisticated theoretical treatments, which are all based on the diffraction model, i.e. the generalization of the

(a)



(b)

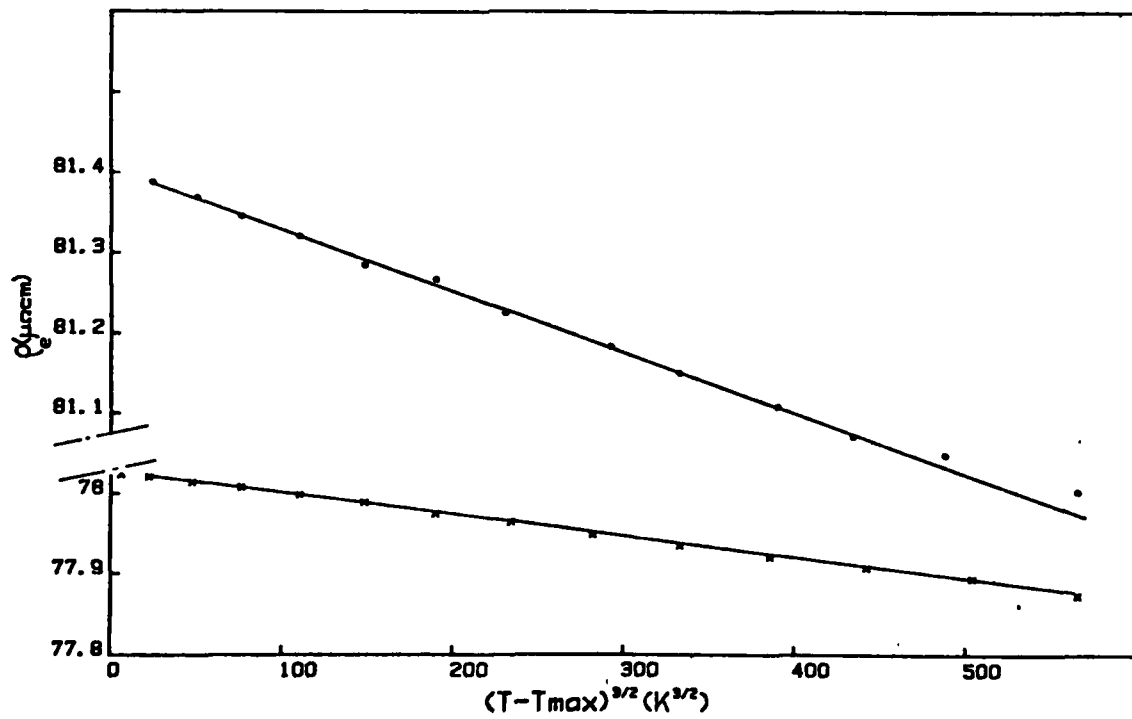


Figure 6 : (a) Maximum in the resistivity versus temperature curves and (b) resistivity as a function of $(T - T_{\max})^{3/2}$ for as-deposited co-evaporated amorphous MgZn alloys . (•) $d_Q = 515 \text{ \AA}$, $x_{\text{Zn}} = 33.5 \text{ at.}\%$; (x) $d_Q = 600 \text{ \AA}$, $x_{\text{Zn}} = 30.5 \text{ at.}\%$.

MgZn _x at. %	ρ_{10K} deposit 20K $\mu\Omega\text{cm}$	ρ_{10K} annealed 300K $\mu\Omega\text{cm}$	ρ_{300K}	$\rho_{\text{max}} / \rho_{300K}$	A (T-T _{max}) ^{3/2} $\mu\Omega\text{cmK}^{-3/2}$	T _{max}	α 10^{-4}K^{-1}
28	78.5	72.5	69.5	1.023	—	45	-1.4
30.5	85	78	76.8	1.015	$3 \cdot 10^{-4}$	80	-0.7
32.5	78	72.7	70.7	1.024	$10 \cdot 10^{-4}$	90	-1.1
33.5	82	81	79.6	1.023	$8 \cdot 10^{-4}$	85	-1.2

Table I : Quantities characteristic of the d.c. electrical resistivity behaviour for co-evaporated amorphous MgZn alloy films with different compositions : ρ values at 10 K before and after annealing, and at 300 K ; ratio of the maximum value to the room temperature value $\rho_{\text{max}} / \rho_{300K}$; slope A of the plot : $\rho = \rho_{\text{max}} - A(T-T_{\text{max}})^{3/2}$; temperature of the maximum T_{max} ; temperature coefficient $\alpha = \frac{1}{\rho} \cdot \frac{d\rho}{dT}$ as determined in the 150-250 K range.

Faber-Ziman theory to amorphous systems, have been proposed recently in order to interpret the results of transport experiments on such low-resistivity amorphous alloys (37-42). They differ in the handling of the different ingredients entering the Faber-Ziman theory, essentially the electron-ion scattering potentials, the partial dynamical structure factors and the vibrational density of states. Some of them take into account the effect of a finite mean free path, either through the concept of phonon ineffectiveness (saturation effects) (37-39), or via the blurring of the Fermi surface (40). All treatments succeed in reproducing the general behaviour of the d.c. electrical resistivity as a function of temperature. This proves that the diffraction model, which is basically a weak-scattering theory, is well adapted to such systems with resistivities smaller than $100 \mu\Omega\text{cm}$. The theoretical values of the resistivity, of the order of $43 \mu\Omega\text{cm}$ for amorphous MgZn alloys (40,41), are in good agreement with the lowest experimental values obtained on quenched samples. As for the exact $\rho(T)$ variation, these ab initio calculations clearly show that it is the result of a rather delicate interplay of structural, electronic and dynamical variables (41); this is particularly the case for the location and relative intensity of the low-temperature maximum, and for the slope in the vicinity of room temperature. All treatments emphasize the dramatic effect of the choice of the potential. On the other hand, factors such as the Fermi wavevector and the packing fraction influence, not only the magnitude of the resistivity, but also the shape of the $\rho(T)$ curve, and could play a role in the scattering of the data relative to differently prepared samples. In spite of the success of these models, some discrepancies with the experimental results concerning for example the composition dependence of the resistivity, or the thermopower behaviour, suggest that the electronic transport properties of the amorphous alloys are not fully taken into account. It may be worth-recalling that actual samples, especially our co-evaporated films, can present structural "defects", or local fluctuations of both chemical and topological short or medium-range, order which may contribute to the electron transport mechanisms and explain for example the observed large values of their resistivity.

4. Optical properties

As already mentioned in section 3, the two types of MgZn films which can be distinguished on the basis of their annealing behaviour (as followed by in situ resistance measurements), also differ by their optical properties. For the first films deposited on silica substrates, the reflectance and transmittance spectra exhibit a structure (a minimum in R and a maximum in T) centred at about $0.95 \mu\text{m}$ as shown in figure 7 in the case of a sample with $d_Q = 259 \text{ \AA}$ and $x_{\text{Zn}} = 26 \text{ at.}\%$. This structure in R and T results in a well-marked shoulder in the optical absorption spectrum ϵ_2/λ , at about 1.25eV , as shown in figure 8 for the same film as before. These features are practically not modified after annealing at 300K (figure 8). On the contrary, for the films deposited subsequently on sapphire substrates, the R and T spectra are smooth in this spectral range, and the optical absorption ϵ_2/λ appears to follow a free-electron-like behaviour, as illustrated in figures 9 and 10 in the case of a film with $d_Q = 600 \text{ \AA}$ and $x_{\text{Zn}} = 30.5 \text{ at.}\%$. From these data, we assume that the films of the second type are truly amorphous MgZn alloys, while the films of the first type are, even just after deposition, probably at least partially phase-separated. This may be due to the fact that the deposition conditions in our first experiments were not optimized, in particular that the evaporation rates were not sufficiently uniform. In the following, we will restrict ourselves to the films of the second type.

We assume that the optical properties of the amorphous MgZn alloys can be represented, at least in the near infra-red, by a nearly-free-electron model. We therefore tried to analyse the experimental complex dielectric constant in terms of the Drude model:

$$\tilde{\epsilon} = P - \frac{\omega_p^2}{\omega(\omega + i/\tau)}$$

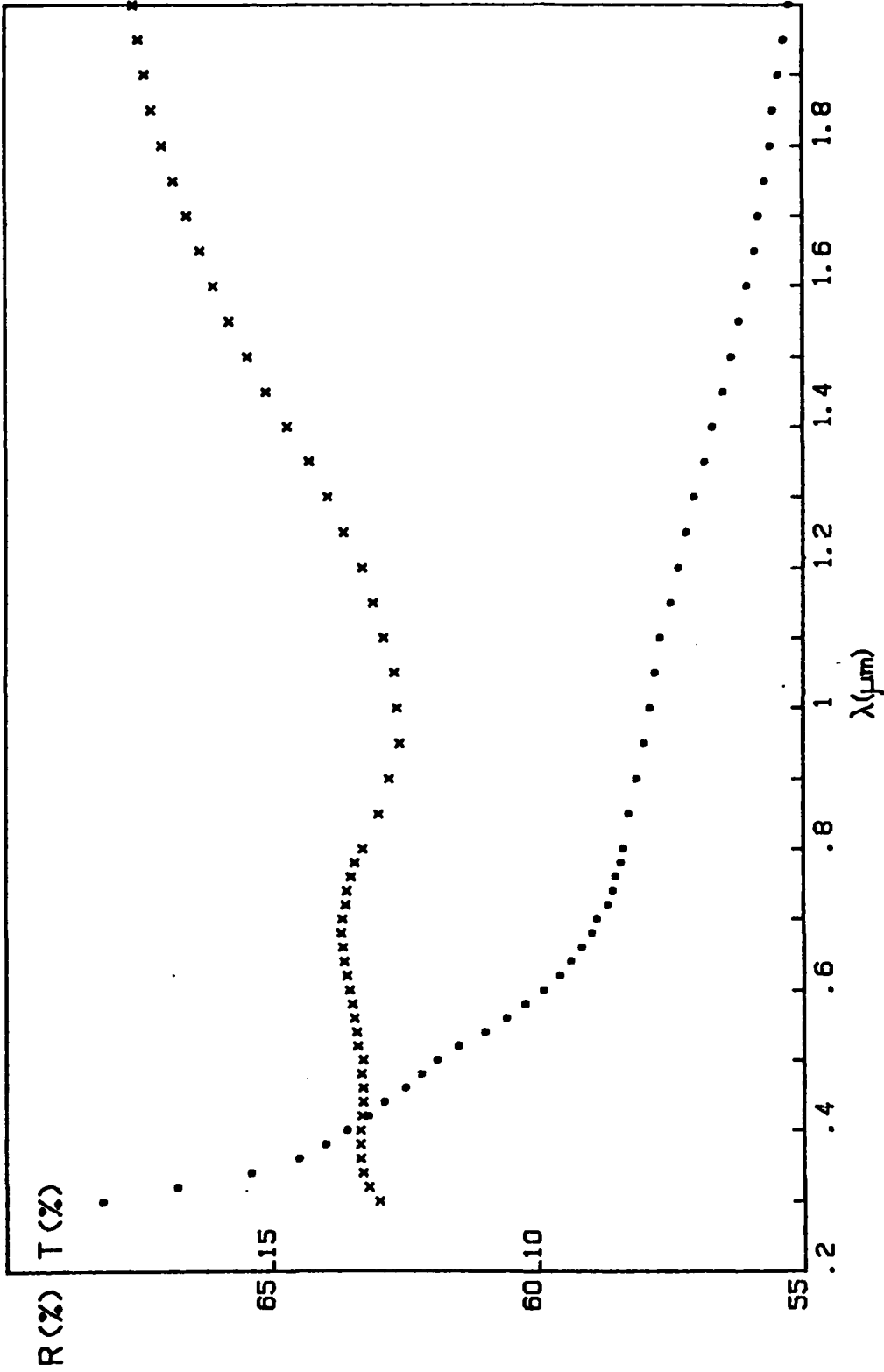


Figure 7 : Reflectance R (x) and transmittance T (•) versus wavelength λ between 0.3 and 2 μm for a co-evaporated amorphous MgZn alloy film ($d_Q = 259 \text{ \AA}$, $x_{Zn} = 26 \text{ at.}\%$) deposited on a silica substrate.

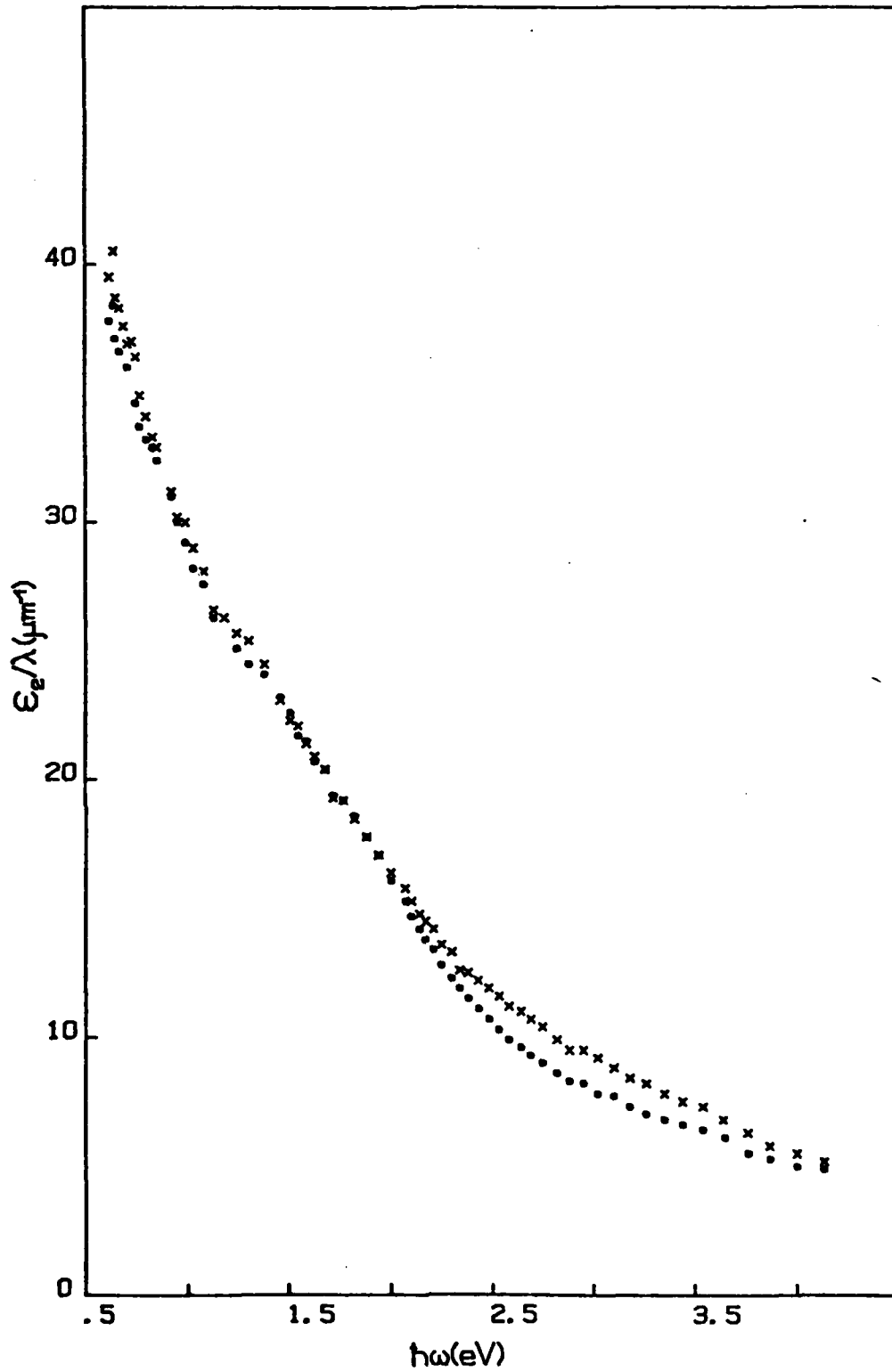


Figure 8 : Optical absorption ϵ_2/λ versus energy $\hbar\omega$ for the same film as in figure 7, as-deposited (x) and annealed at room temperature (•).

where $\omega_p = \left(\frac{4\pi N_{\text{eff}} e^2}{m_0} \right)^{1/2}$ is the plasma frequency of the nearly-free-electron gas with an effective number per unit volume N_{eff} and an optical effective mass m_0 , and τ_0 is the optical relaxation time of the conduction electrons, assumed to be independent on frequency. The real term P , which is equal to: $1 + (\epsilon_{\infty} - 1) + \delta\epsilon_1^b$, accounts for the core polarization ($\epsilon_{\infty} - 1$), and for the possible contribution of interband transitions occurring at higher energies:

$$\delta\epsilon_1^b = \frac{2}{\pi} \int_{\omega_p}^{\infty} \frac{\omega' \cdot \epsilon_2(\omega')}{\omega'^2 - \omega^2} d\omega'$$

this contribution can be considered as a constant for $\omega \ll \omega_b$, ω_b being the onset of interband transitions. The Drude formula can thus be written as a function of wavelength:

$$\epsilon_1 = P - \frac{\lambda^2}{\lambda_0^2} \cdot \frac{1}{1 + (\lambda/\lambda_{\tau})^2}$$

$$\epsilon_2 = \frac{\lambda^3}{\lambda_0^2 \lambda_{\tau}} \cdot \frac{1}{1 + (\lambda/\lambda_{\tau})^2}$$

with $\lambda_0 = 2\pi c/\omega_p$ and $\lambda_{\tau} = 2\pi c\tau_0$.

We used a least square curve fitting procedure, either directly on the (R,T) data, or on the computed (ϵ_1, ϵ_2) data, taking $\lambda_0, \lambda_{\tau}$ and P as adjustable parameters. Due to the problems encountered in the determination of the actual film thickness, we employed in the computations both the average mass thickness d_0 and the thickness d_{alloy} corresponding to a density larger than the average Mg/Zn density by 5% as explained in section 2. We also considered the thickness d as an additional adjustable parameter in the curve-fitting procedure (in this case, we used only the (R,T) data). Fits between the data and the Drude model have been tried over spectral ranges of increasing width, from 2 or 2.5 μm (depending on the accuracy of the measurement in the low-energy part of the spectrum) to 1.2, 1, 0.8, 0.6 and 0.4 μm respectively. The results obtained in the case of a film with $d_0 = 600 \text{ \AA}$ ($d_{\text{alloy}} = 555 \text{ \AA}$) and $x_{\text{Zn}} = 30.5 \text{ at.}\%$, are summarized in Table II. We have used, either the (R,T),

Fit no	Fit range	d (\AA)	$\lambda_0(\mu\text{m})$	$\lambda_\tau(\mu\text{m})$	P	Σ
1	(R-T) 1.2-2.0 μm (λ_0 - λ_τ -P)	<u>600</u>	0.159	1.99	1.0	$4 \cdot 10^{-6}$
2	(R-T) 0.6-2.0 μm (λ_0 - λ_τ -P)	<u>600</u>	0.156	1.85	0.186	$9.2 \cdot 10^{-6}$
3	(R-T) 0.4-2.0 μm (λ_0 - λ_τ -P)	<u>600</u>	0.147	1.71	0.457	$1.2 \cdot 10^{-5}$
4	(R) 0.6-2.0 μm (λ_0 - λ_τ -P)	<u>600</u>	0.145	1.64	0.057	$1.8 \cdot 10^{-5}$
5	(R-T) 0.8-2.0 μm (λ_0 - λ_τ -P-d)	530	0.142	1.68	0.030	$9.3 \cdot 10^{-6}$
6	(R-T) 0.8-2.0 μm (λ_0 - λ_τ -d)	552	0.147	1.78	<u>1.0</u>	$8 \cdot 10^{-6}$
7	(R-T) 0.8-2.0 μm (λ_0 - λ_τ -P)	<u>555</u>	0.149	1.75	-0.05	$8 \cdot 10^{-6}$
8	(R-T) 0.8-2.0 μm (λ_0 - λ_τ)	<u>555</u>	0.148	1.79	<u>1.0</u>	$1 \cdot 10^{-5}$
9	(R-T) 0.8-2.0 μm (λ_τ -P-d)	391	<u>0.1035</u>	1.15	-0.2	$6 \cdot 10^{-6}$

Table II : Results of several fits of the experimental reflectance (R) and transmittance (T) data with the Drude model for an amorphous MgZn alloy film with $x_{\text{Zn}} = 30,5$ at.% and $d_0 = 600 \text{ \AA}$ ($d_{\text{alloy}} = 555 \text{ \AA}$). The fit number, the spectral range used for the fit and the adjustable parameters, the values of the thickness d , plasma wavelength λ_0 , relaxation wavelength λ_τ and polarization term P , and the root mean square deviation per point Σ are indicated in each case. Any parameter which has been fixed at a given value in a particular fit is underlined. The asterisk points out the parameters which happen to be highly correlated.

or only the (R) data ; the root mean square deviation per point is also indicated. Our program gives the asymptotic correlation matrix of the parameters, which allows to estimate the coupling of the different parameters. Figure 9 shows a comparison between the experimental (R,T) values and the values corresponding to the Drude model, computed with the parameters deduced from the fit (2). Figure 10 presents a comparison between the experimental (ϵ_1, ϵ_2) values determined from the (R,T) data with $d = d_Q$, and the (ϵ_1, ϵ_2) values corresponding to the Drude model, computed with the parameters deduced from fits (2) and (3) respectively. Figure 11 shows a similar comparison between the experimental and model (ϵ_1, ϵ_2) values, the thickness value being in this case that obtained by fit (5) with four parameters, $\lambda_0, \lambda_\tau, P$ and d , i.e. $d = 530 \text{ \AA}$. When examining all these results, one can make the following remarks :

a) the optical data follow remarkably well the nearly-free-electron Drude model with a constant relaxation time, from the lowest energies (0.5-0.6 eV) up to about 1.8 eV. At higher energies, the optical absorption ϵ_2/λ takes slightly larger values than the model ones, while the deviation remains very small for ϵ_1 . It is therefore wiser to restrict the fitting procedure to the spectral range (0.5-1.8 eV), i.e. (2.5-0.7 μm). The three parameters λ_0, λ_τ and P are not strongly correlated and can easily be determined ; however, the parameter P , the value of which is expected to be close to, but larger than 1, often takes very small, or even negative values. If the fit domain is restricted to low energies (for example 2-1.2 μm), P on the contrary takes larger values. Fixing P at a value equal to 1 or 2 does not however modify appreciably the values of the two other parameters, λ_0 and λ_τ (see fits (7) and (8)).

b) it proved possible in a few cases to determine λ_0, λ_τ and P from the (R) data alone (see fit (4)), which may be interesting for thick films, the transmittance of which becomes extremely small and difficult to measure. However, the parameters λ_0 and λ_τ are then strongly correlated.

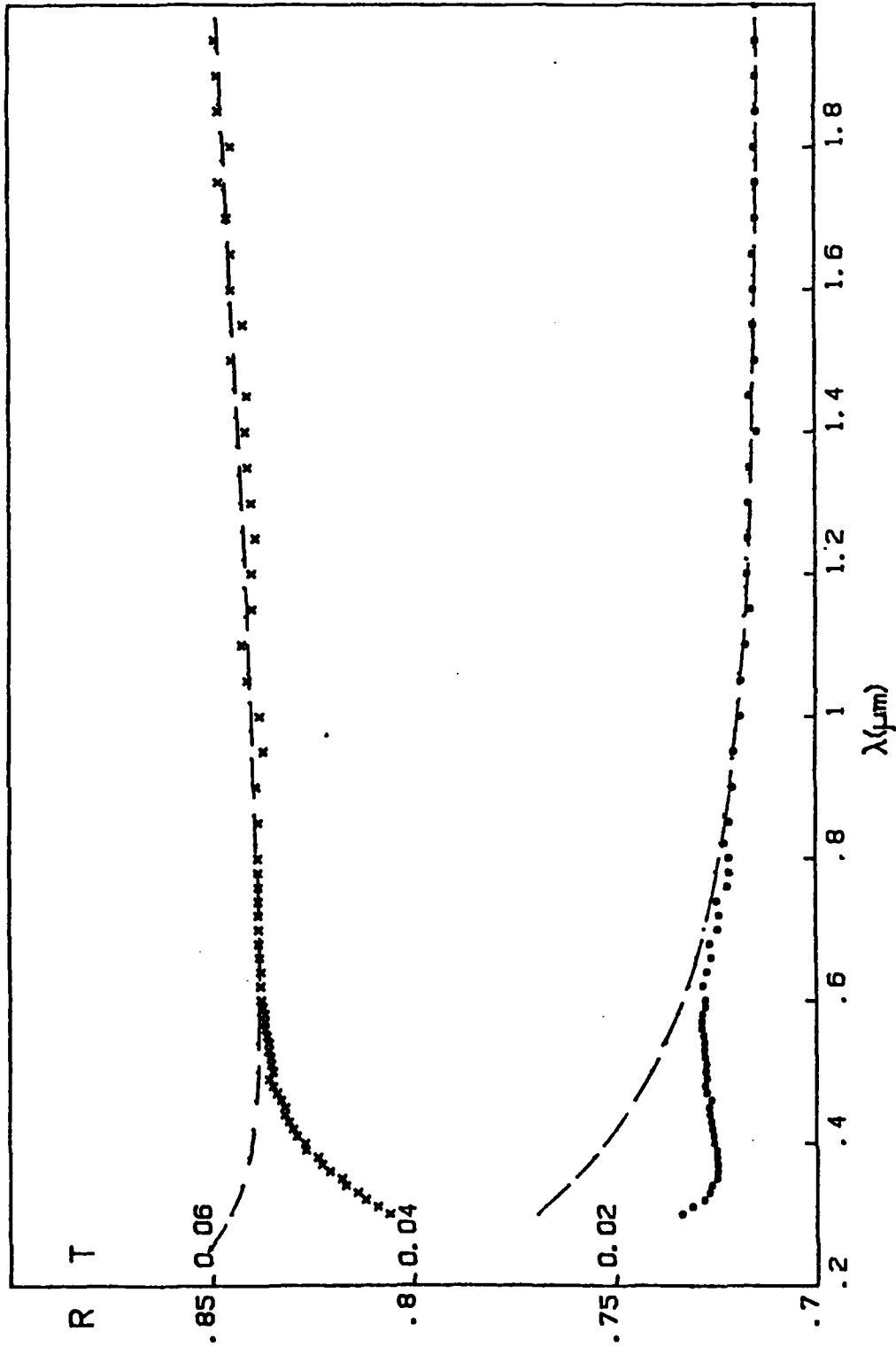


Figure 9 : Reflectance R (\times) and transmittance T (\bullet) versus wavelength λ between 0.3 and $2 \mu\text{m}$ for a co-evaporated amorphous Mg/Zn alloy film ($d_0 = 600 \text{ \AA}$, $x_{\text{Zn}} = 30.5 \text{ at.}\%$) deposited on a sapphire substrate ; the dashed curve corresponds to the Drude fit (2) (see Table II).

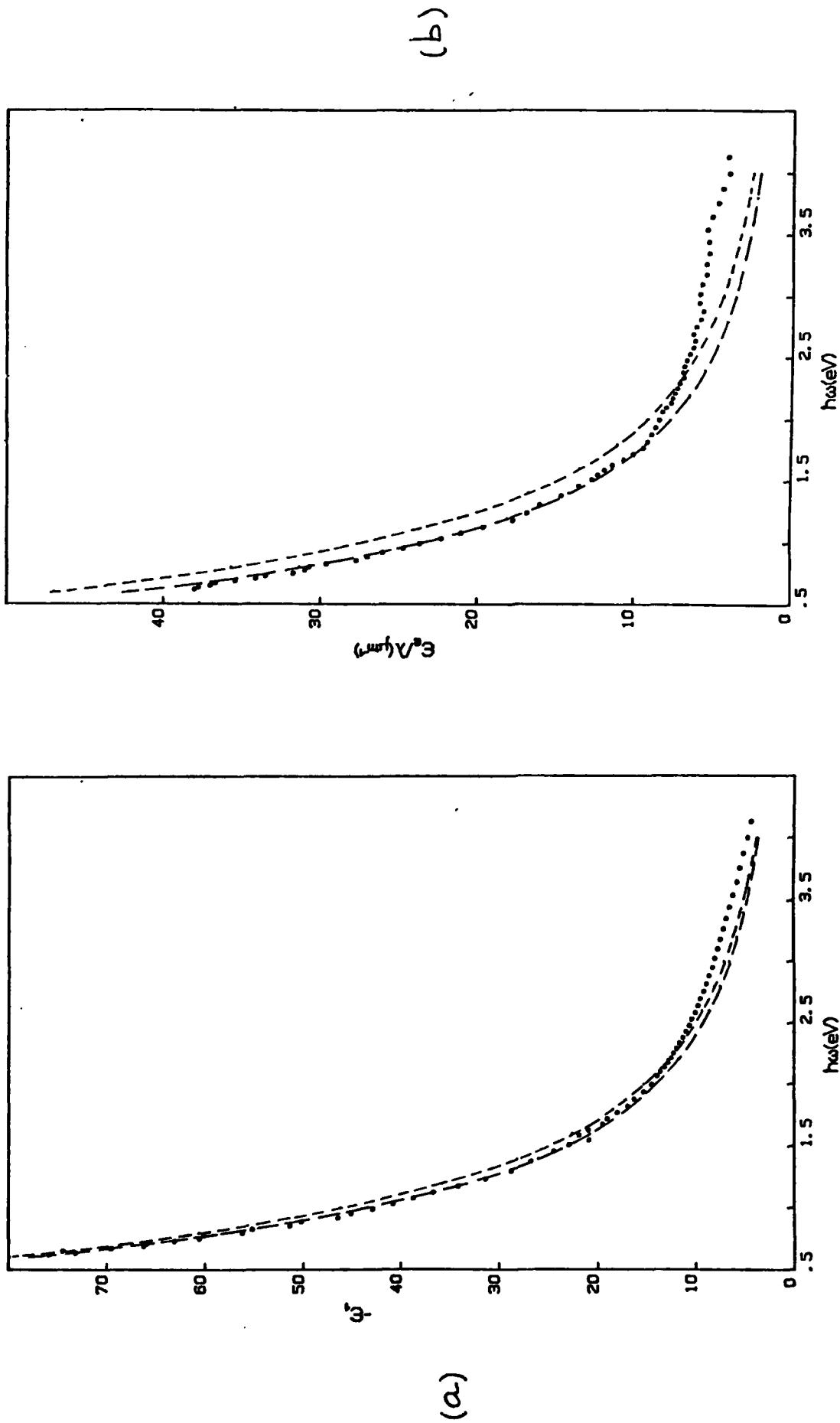
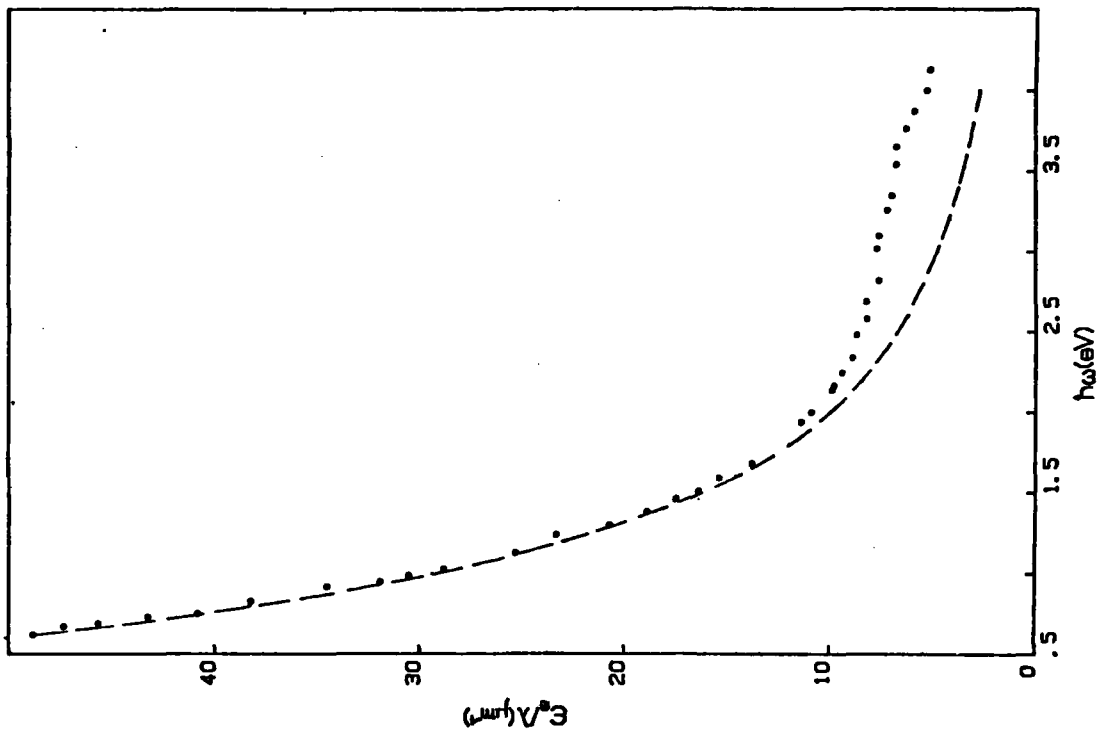
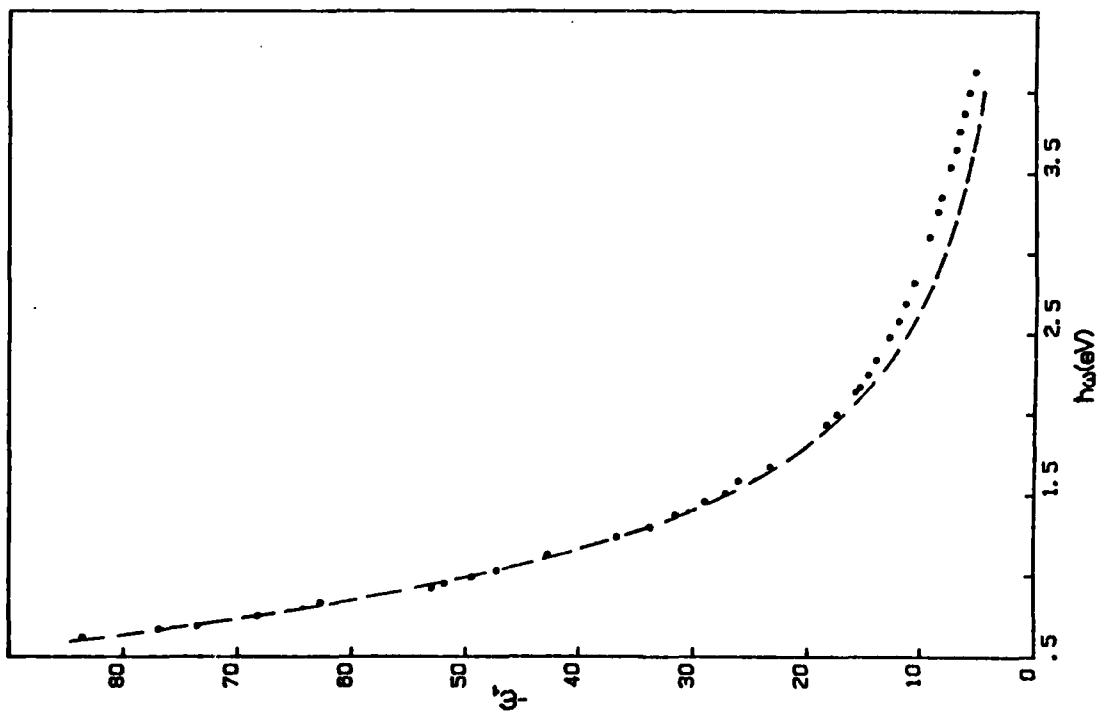


Figure 10 : Real part of the dielectric constant ϵ_1 (a) and optical absorption ϵ_2/λ (b) versus energy for the same film as in figure 9, as computed with $d = dQ = 600 \text{ \AA}$; the long-dashed and short-dashed curves correspond to the Drude fits (2) and (3) respectively (see table II).



(b)



(a)

Figure 11 : Real part of the dielectric constant ϵ_1 (a) and optical absorption ϵ_2/λ (b) versus energy for the same film as in figures 9 and 10, as computed with d equal to the value deduced from the Drude fit (5), 530 Å (see Table II) ; the dashed curves correspond to this Drude fit.

c) the determination of the thickness from the optical data only, by considering it as an adjustable parameter in the Drude fitting procedure, is not possible in all cases, because λ_0 becomes strongly correlated both with d and with λ_τ . For the film considered here, we succeeded in determining d , P being taken both as an adjustable (fit (5)) or fixed (fit (6)) parameter. The obtained values are clearly different from d_Q , and have been used to define d_{alloy} , as explained in section 2. It may be worth-noticing that the values of the parameters λ_0 and λ_τ deduced from the (R) data alone using the thickness d_Q are of the same order of magnitude as those deduced from the (R, T) data using, not this "wrong" thickness d_Q , but the "more correct" thickness d_{alloy} . This can simply mean that the reflectance is less sensitive to the film thickness than the transmittance.

d) we have verified that the values of the parameters λ_0 and λ_τ obtained by a computer-fitting procedure as explained above are consistent with those determined graphically by the relations, easily deduced from the Drude expression :

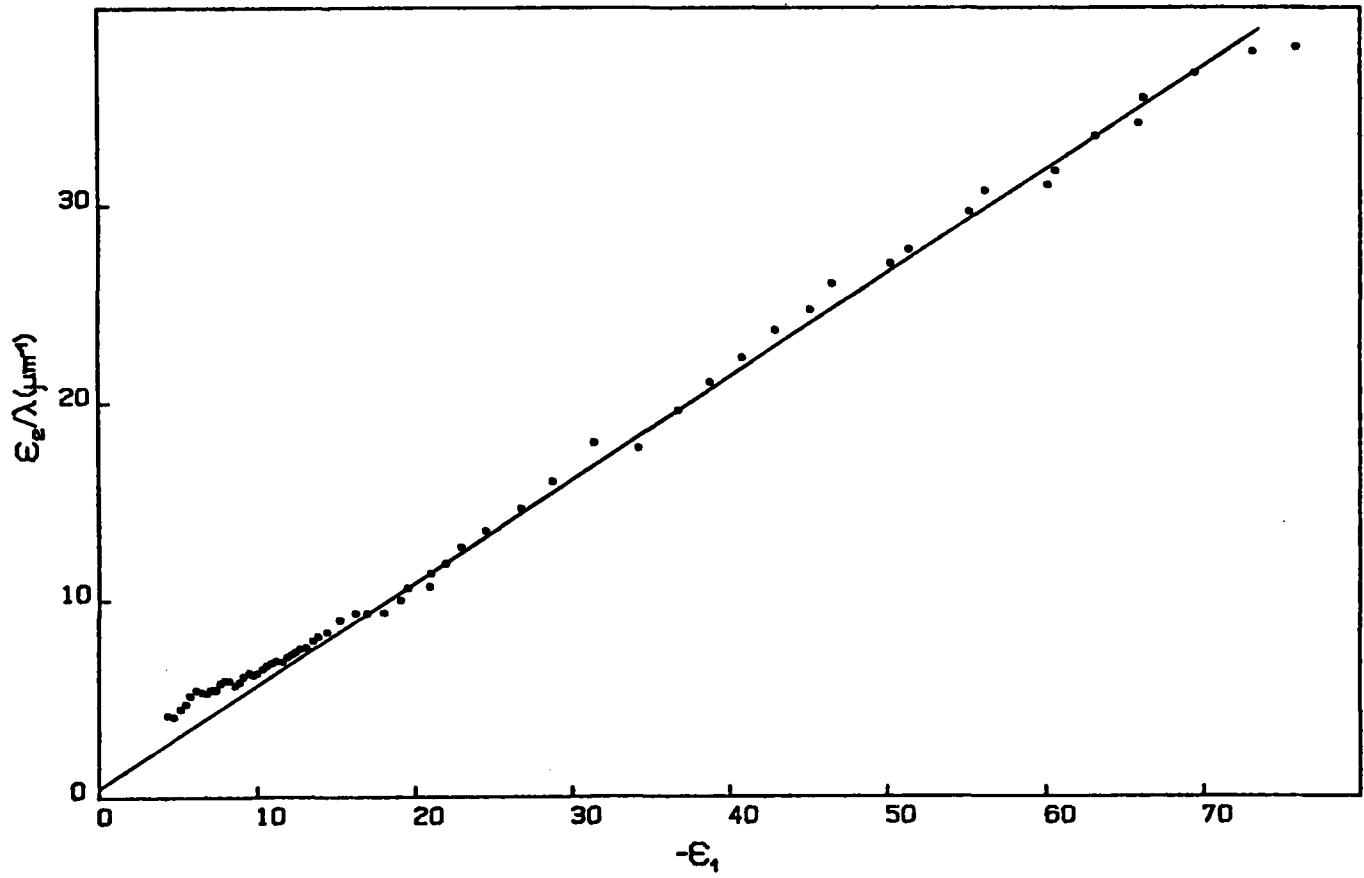
$$\frac{\epsilon_2}{\lambda} = \frac{1}{\lambda_\tau} (P - \epsilon_1)$$

which gives λ_τ , then P , and :

$$\left(\frac{\epsilon_2}{\lambda}\right)^{-1} = \lambda_0^2 \lambda_\tau \cdot \lambda^{-2} + \frac{\lambda_0^2}{\lambda_\tau}$$

which gives λ_0 . The straight lines obtained when plotting ϵ_2/λ versus $(-\epsilon_1)$, and $(\epsilon_2/\lambda)^{-1}$ versus λ^{-2} for the same film discussed above (with $d_Q = 600 \text{ \AA}$) are presented in figure 12. The corresponding parameter values are : $\lambda_0 \approx 0.155 \text{ \mu m}$, $\lambda_\tau \approx 1.90 \text{ \mu m}$, $P \approx 1$.

(a)



(b)

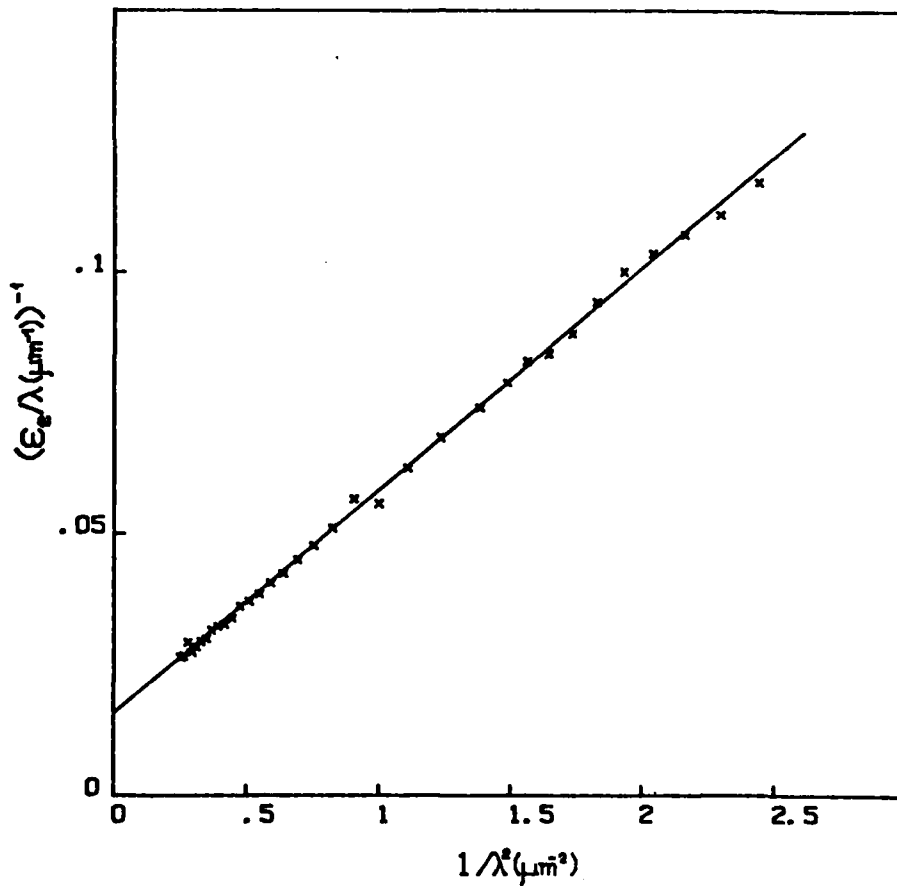


Figure 12 : Graphical test of the Drude model for the same film as in figures 9-11, using $d = d_0 = 600 \text{ \AA}$: (a) ϵ_2/λ versus $(-\epsilon_1)$; (b) $(\epsilon_2/\lambda)^{-1}$ versus λ^{-2} .

The values of the parameters λ_0 and λ_τ (as well as the corresponding $\hbar\omega_p$ and \hbar/τ_0 values) determined for amorphous MgZn alloys with Zn concentrations comprised between 28 and 33.5 at.%, are summarized in Table III and figure 13. Only the values corresponding to the assumed actual film thickness d_{alloy} have been retained in the table, but the figure presents the results obtained with both thickness values d_Q and d_{alloy} . We have also reported in Table III the values of the average effective number of conduction electrons per atom n_{eff} computed from λ_0 by assuming an optical effective mass equal to the free electron mass (these values are displayed in figure 14), as well as the values of the ratio of the optical effective mass to the free-electron mass m_0/m computed from λ_0 by assuming an average effective number of conduction electrons per atom equal to 2, which is the common valency of both constituents. We have eventually indicated, both in Table III and in figure 3, the values of the "optical resistivity" ρ_0 , defined from the optical parameters by the expression :

$$\rho_0 = \frac{m_0}{N_{\text{eff}} e^2 \tau_0} = \frac{2}{c} \frac{\lambda_0^2}{\lambda_\tau}$$

These results call for the following comments :

a) the values of λ_0 are significantly larger than those expected from a free-electron model in which each constituent would contribute two electrons to the alloy conduction band, with an optical effective mass equal to the free-electron mass ; for example for $x_{\text{Zn}} \approx 30$ at.%, the predicted free-electron value of λ_0 should be of the order of $0.107 \mu\text{m}$, while the experimental value is of the order of $0.150 \mu\text{m}$. The difference definitely exceeds any possible experimental uncertainty. If we try to fit the optical data with the Drude model, with λ_0 fixed at the free-electron value and d taken as an adjustable parameter (see Table II), the obtained d value is unreasonably too small : $d = 391 \text{ \AA}$, compared to $d_Q = 600 \text{ \AA}$ in the case of the film corresponding to Table II. This discrepancy between the experimental λ_0 value and the value predicted by a simple free-electron model

MgZn	x_{Zn} (at. %)	$\lambda_0(\mu m)$	$\hbar\omega_p$ (eV)	Γ_{off}	m_0/m	$\lambda_e(\mu m)$	\hbar/τ (eV)	$\rho(\mu cm)$
9	28	0.148	8.38	0.98	2.04	1.88	0.66	77.7
5	30.5	0.148	8.38	0.97	2.05	1.78	0.70	82.0
7	32.5	0.142	8.73	1.05	1.90	2.02	0.61	66.5
6	33.5	0.140	8.86	1.08	1.85	1.53	0.81	85.4

Table III : Values of the free-electron parameters as deduced from the Drude analysis of the optical data for amorphous MgZn alloys with different compositions (see text for the definitions).

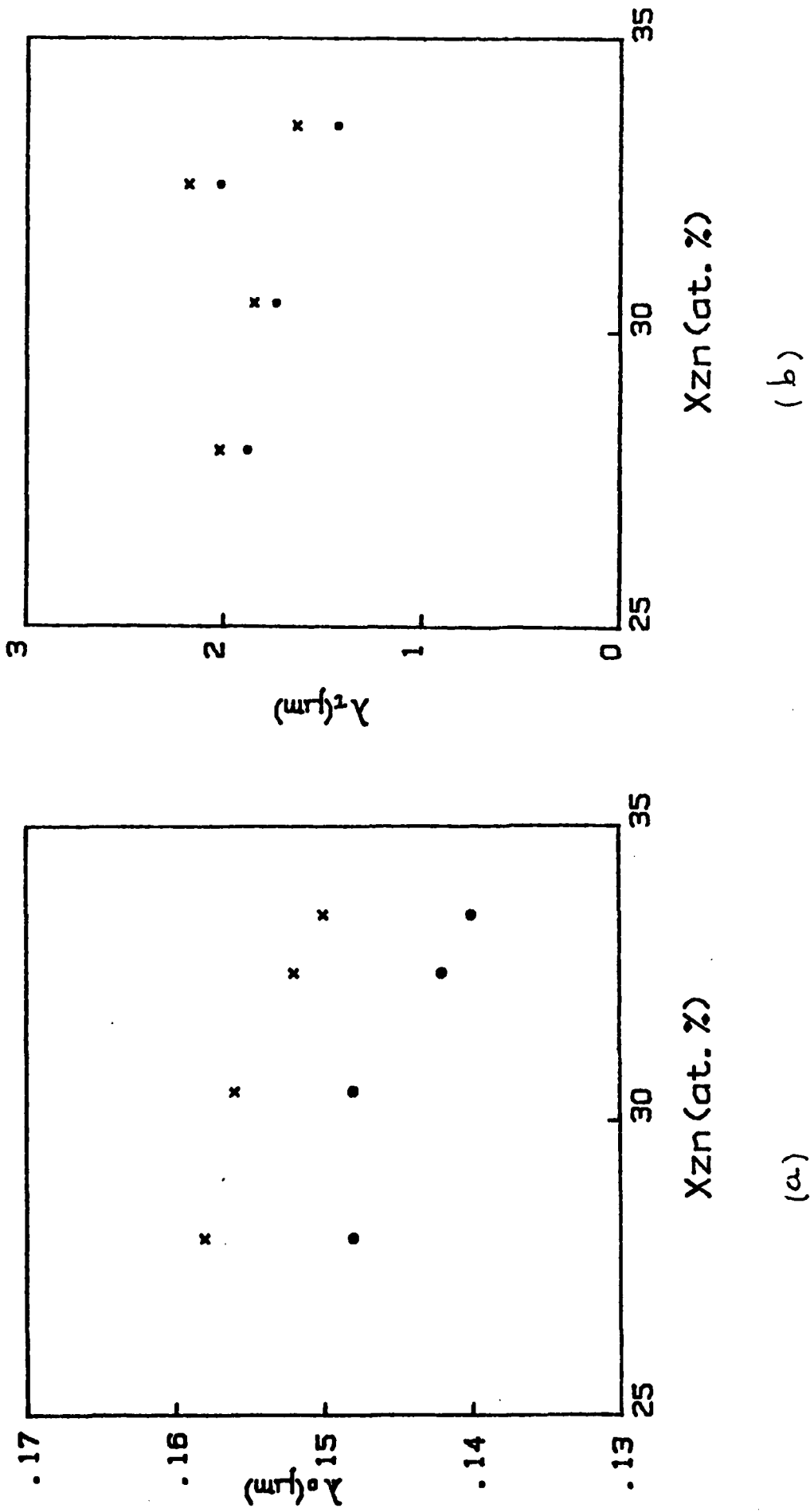


Figure 13 : Values of the plasma wavelength λ_p (a) and of the relaxation wavelength λ_T (b) versus atomic Zn concentration X_{Zn} for co-evaporated amorphous MgZn alloy films, as deduced from the Drude analysis of the optical data, with $d = d_Q$ (x) and $d = d_{alloy}$ (o).

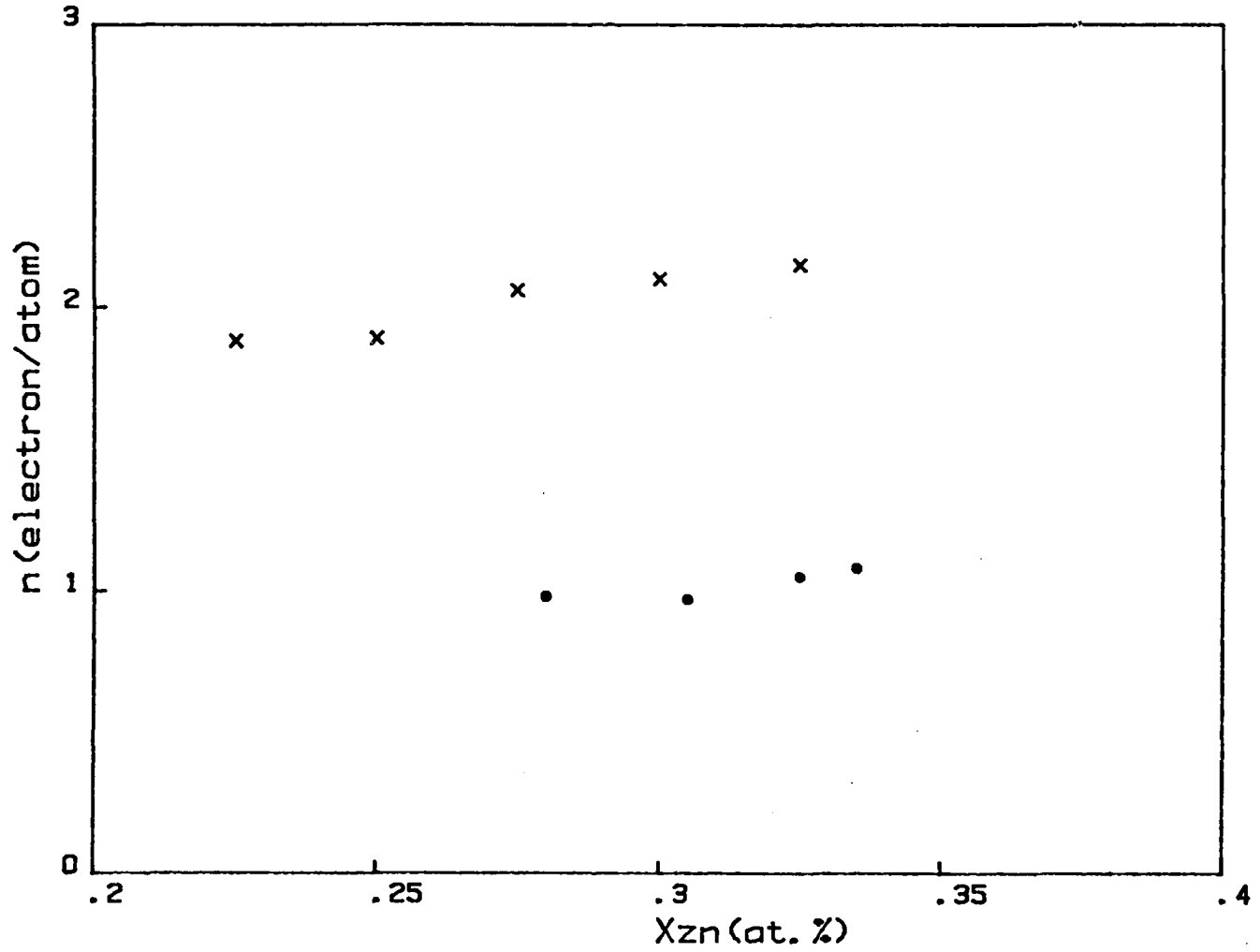


Figure 14 : Average number of conduction electrons per atom n versus atomic Zn concentration x_{Zn} for amorphous Mg/Zn alloys : (x) deduced from Hall constant measurements on quenched alloys (ref.12) ; (•) deduced from the Drude analysis of the optical data obtained on co-evaporated alloy films (with an effective mass equal to the free electron mass).

can be interpreted as due, either to a value of the effective average number of conduction electrons per atom, as deduced from the optical properties, much smaller than 2, or to an enhancement of the optical effective mass of the conduction electrons with respect to the free electron mass. The first interpretation is in contradiction with the results of Hall constant measurements on quenched amorphous MgZn alloys (12), which give an average number of conduction electrons per atom of the order of 2, varying only slightly with composition (these values are also reported in figure 14), as well as with those of Compton profile (26) and electronic specific heat coefficient (24) experiments, which both yield a Fermi wavevector k_F in good agreement with the predicted free-electron value. The second interpretation, in terms of optical mass enhancement, has previously been chosen to explain similar discrepancies observed between the optical results and the predictions of a free-electron model, in the case of free-electron-like amorphous SnCu and SnAu alloys (28). The ratio m_0/m was found to be comprised between about 1.6 and 1.7 for SnCu, between 1.8 and 1.4 for SnAu, for noble metal concentrations varying from 20 to 80 at.%

b) the values of λ_τ are comprised between 1.5 and 2.5 μm , which corresponds to \hbar/τ values comprised between 0.8 and 0.5 eV. These values seem to depend rather sensitively on the peculiar film structure, so that their variation with the alloy composition cannot be clearly established. The optical relaxation time in amorphous MgZn alloys is significantly larger than in similarly prepared amorphous AuGe and AgGe alloys (29), or amorphous AuSn and CuSn alloys (28), which is consistent with the lower resistivities of these alloys, and can probably be traced back to the fact that their conduction electrons have essentially an s and p character. The corresponding mean free path is of the order of 15-20 \AA , which is appreciably larger than the interatomic distances, so that a free-electron model can be justified.

c) the optical resistivity ρ_0 deduced from the optical parameters λ_0 and λ_τ , is in all cases of the same order of magnitude as the

d.c. electrical resistivity ρ_e . This is an additional argument in favour of the use of a free-electron model for the analysis of the optical data. The difference between ρ_o and ρ_e , which varies from sample to sample, can probably only be attributed to experimental uncertainties on the optical data.

5. Conclusion

We have succeeded in preparing amorphous MgZn alloys in the form of thin films, by co-evaporation under ultra-high vacuum on sapphire substrates maintained at low temperature (10K), for Zn concentrations ranging from 25 to 35 at.%. The samples can be annealed in situ up to room temperature while remaining amorphous ; they crystallize at about 350K, like quenched bulk alloys. The d.c. electrical resistivity and the optical properties between 0.6 and 4eV of these amorphous alloy films have been investigated in situ in order to avoid contamination. The behaviour of their resistivity versus temperature is found to be similar to the one reported for quenched bulk alloys, with only small differences in the details of the curves, i.e. in the location of the maximum, slope of the high-temperature part, etc... and it can be well interpreted in the framework of the diffraction model. However, the absolute values of the resistivity are significantly higher than those for quenched alloys. This suggests that thin films, even after annealing at room temperature, contain "defects", probably related to medium-range inhomogeneities, which may contribute to the electron scattering. As for the optical properties of the amorphous alloy films, although we encountered some difficulties in the determination of the film thickness, their analysis unambiguously shows that the complex dielectric constant follows quite well the free-electron Drude model, at least at low energies up to about 1.8 eV. The "optical resistivity" deduced from the optical conduction electron parameters is in all cases very close to the d.c. electrical resistivity. The optical relaxation time \hbar/τ_o is comprised between 0.5 and 0.8 eV and seems to be sensitive to the film structure more than to its composition ;

\hbar/τ_0 is smaller in these amorphous alloys between two simple metals than in other amorphous free-electron-like alloys involving a noble metal. The values of the average optical effective number of conduction electrons per atom raise a problem, since they are definitely smaller than the value expected from the free-electron model, i.e. 2, and indeed found in Hall effect experiments. This discrepancy could indicate that the alloy conduction band deviates strongly from a free-electron band. It is worth-recalling that photoemission and soft-X-ray emission experiments performed on the parent amorphous alloys CaAl have revealed unexpected structures in the valence band density of states, as well as modifications of the Al p partial density of occupied states with respect to pure Al (43). Computations on $\text{Ca}_{0.75}\text{Al}_{0.25}$ with the Cu_3Au structure have on the other hand shown a splitting of the valence band into two parts. The Al partial density of states is clearly separated into s states and p states at high and low binding energies respectively, due to the reduced overlap of the orbitals from nearest neighbour like-atoms. As for the Ca states, they are subject to strong hybridization, which also leads to a splitting. We intend to verify whether such effects exist in amorphous MgZn alloys, as soon as we succeed in protecting our samples from oxidization. Interband transitions between occupied and unoccupied states could then be responsible for the deviation between the experimental complex dielectric constant and the Drude model observed at high energies (>1.8 eV).

References

1. J. HAFNER and L. VON HEIMENDAHL, Phys. Rev. Lett. 42, 386 (1979).
2. J. HAFNER, J. Physique 41, C8-139 (1980).
3. J. HAFNER, Phys. Rev. 21, 406 (1980).
4. S.M. MUJIBUR RAHMAN, Z. Phys. B 45, 307 (1982).
5. J.M. ZIMAN, Phil. Mag. 6, 1013 (1961).
6. T.E. FABER and J.M. ZIMAN, Phil. Mag. 11, 153 (1965).
7. T.E. FABER, Theory of liquid metals (Cambridge University Press, London, 1972).
8. G. BAYM, Phys. Rev. A 135, 1691 (1964).
9. K. FROBÖSE and J. JÄCKLE, J. Phys. F 7, 2331 (1977).
10. J. JÄCKLE and K. FROBÖSE, J. Phys. F 9, 967 (1979).
11. A. CALKA, M. MADHAVA, D.E. POLK, B.C. GIESSEN, H. MATYJA and J. VANDER SANDE, Scripta Metall. 11, 65 (1977).
12. T. MATSUDA and U. MIZUTANI, in Proc. 4th Int. Conf. Rapidly Quenched Metals (Sendai, 1981) p. 1315.
13. J.J. HAUSER and J. TAUC, Phys. Rev. B 17, 3371 (1978).
14. T. MIZOGUCHI, N. SHIOTANI, U. MIZUTANI, T. KUDO and S. YAMADA, J. Physique 41, C8-183 (1980).
15. E. NASSIF, P. LAMPARTER, W. SPERL and S. STEEB, Z. Naturforsch. 38a, 142 (1983).
16. L. VON HEIMENDAHL, J. Phys. F 9, 161 (1979).
17. H. RUDIN, S. JOST and H.J. GÜNTHERODT, J. Non-Cryst. Sol. 61/62, 291 (1984).
18. N. SHIOTANI, H. NARUMI, H. ARAI, K. WAKATSUKI, Y. SASA and T. MIZOGUCHI, in Proc. 4th. Int. Conf. Rapidly Quenched Metals, eds. T. MASUMOTO and K. SUSUKI (Japan Inst. Metals, 1981) p. 667.
19. M. ITC, H. IWASAKI, N. SHIOTANI, H. NARUMI, T. MIZOGUCHI and T. KAWAMURA, J. Non-Cryst. Sol. 61/62, 303 (1984).
20. J. HAFNER, E. GRATZ and H.J. GÜNTHERODT, J. Physique 41, C8-512 (1980).
21. T. MATSUDA and U. MIZUTANI, J. Phys. F 12, 1877 (1982).

22. M.N. BAIBICH, W.B. MUIR, Z. ALTOUNIAN and TU GUO-HUA, Phys. Rev. B 26, 2963 (1982).
23. G. FRITSCH, J. WILLER, A. WILDERMUTH and E. LUSCHER, J. Phys. F 12, 2965 (1982).
24. U. MIZUTANI and T. MIZOGUCHI, J. Phys. F 11, 1385 (1981).
25. B.C. GIESSEN, A. CALKA, R. RAMAN and D.J. SELLMYER, in Proc. 2nd. Int. Symp. Amorphous Magnetism, eds. R.A. LEVY and R. HASEGAWA (Plenum, New-York, 1977) p. 197.
26. N. SHIOTANI, N. SAKAI, H. SEKIZAWA and T. MIZOGUCHI, J. Phys. Soc. Japan 50, 828 (1981).
27. E. HAUSER, R.J. ZIRCKE, J. TAUC, J.J. HAUSER and S.R. NAGEL, Phys. Rev. Lett. 40, 1733 (1978) ; Phys. Rev. B 19, 6331 (1979).
28. D. KORN and H. PFEIFLE, J. Phys. F 9, 1175 (1979).
29. M.L. THEYE, V. NGUYEN VAN and S. FISSON, Phil. Mag. B 47, 31 (1983).
30. V. NGUYEN VAN and S. FISSON, Rev. Phys. Appl. 13, 155 (1978).
31. J.P. DUPIN, private communication.
32. H. KIESSIG, Annln Physik 10, 769 (1931).
33. F. ABELES, in Progress in Optics, ed. E. WOLF (North-Holland, Amsterdam, 1963) p. 251.
34. F. ABELES and M.L. THEYE, Surf. Sci. 5, 325 (1966).
35. T. MIZOGUCHI, H. NARUMI, N. AKUTSU, N. WATANABE, N. SHIOTANI and M. ITO, J. Non-Cryst. Sol. 61/62, 285 (1984).
36. L.V. MEISEL and P.J. COTE, Phys. Rev. B 17, 4652 (1978).
37. L.V. MEISEL and P.J. COTE, Phys. Rev. B 27, 4617 (1983).
38. P.J. COTE and L.V. MEISEL, J. Non-Cryst. Sol. 61/62, 1167 (1984).
39. L.V. MEISEL and P.J. COTE, J. Non-Cryst. Sol. 61/62, 1307 (1984).
40. J. LAAKKONEN and R.M. NIEMINEN, J. Phys. F 13, 2265 (1983).
41. J. HAFNER, to appear in J. Non-Cryst. Sol.
42. J. HAFNER, to appear in J. Phys. F
43. S.R. NAGEL, U.M. GUBLER, C.F. HAGUE, J. KRIEG, R. LAPKA, P. OELHAFEN, H.J. GÜNTHERODT, J. EVERS, A. WEISS, V. L. MORUZZI and A.R. WILLIAMS, Phys. Rev. Lett. 49, 575 (1982).